MODELLING CRYSTALLIZATION FOULING IN LIQUID-TO-AIR MEMBRANE ENERGY EXCHANGERS

A Thesis Submitted to the College of Graduate and Postdoctoral Studies

In Partial Fulfillment of the Requirements

For the Degree of Master of Science

In the Department of Mechanical Engineering

University of Saskatchewan

Saskatoon

By

Alireza Razmavar

PERMISSION TO USE

In presenting this thesis in partial fulfillment of the requirements for a Postgraduate degree from the University of Saskatchewan, I agree that the Libraries of this University may make it freely available for inspection. I further agree that permission for copying of this thesis in any manner, in whole or in part, for scholarly purposes may be granted by the professors who supervised my thesis work or, in their absence, by the Head of the Department or the Dean of the College in which my thesis work was done. It is understood that any copying, publication, or use of this thesis or parts thereof for financial gain shall not be allowed without my written permission. It is also understood that due recognition shall be given to me and to the University of Saskatchewan in any scholarly use which may be made of any material in my thesis.

Requests for permission to copy or to make other use of material in this thesis in whole or in part should be addressed to:

Head of the Department of Mechanical Engineering

University of Saskatchewan

Saskatoon, Saskatchewan S7N 5A9

Canada

OR

Dean of College of Graduate and Postdoctoral Studies

University of Saskatchewan

116 Thorvaldson Building, 110 Science Place

Saskatoon, Saskatchewan S7N 5C9

Canada

ABSTRACT

Micro-porous membranes are used in membrane-based separation processes to separate water from an aqueous solution. Liquid-to-air membrane energy exchangers (LAMEEs) use membranes to control humidity and temperature in heating, ventilation and air-conditioning (HVAC) systems. A semi-permeable hydrophobic membrane is used in LAMEEs to separate an air stream from an aqueous solution stream while allowing simultaneous heat and moisture transfer between the streams. However, the membrane of LAMEEs may be subjected to crystallization fouling under some operating conditions which impacts performance. The primary goal of this thesis is to establish a model for LAMEEs that can predict the crystallization fouling rate, decline in moisture transfer flux due to fouling, and the operating/design conditions where fouling is likely to occur.

In this thesis, a semi-empirical model is developed to predict crystallization fouling of the membrane in LAMEEs. The solution concentration at solution-membrane interface is determined analytically using mass and energy balance equations, while the fouling (i.e., blockage of the membrane pores) is predicted using an empirical equation from the literature. As the fouling progresses and more of the membrane pores are blocked, moisture transfer flux through the membrane reduces. The model is validated with experimental data available in the literature and is used to determine the effect of design and operating parameters on the fouling rate. The model is also used to estimate the time when the moisture transfer flux declines to a specific value (e.g. 50% reduction) which is helpful in determining the membrane cleaning frequency.

Then, the model is used to predict the conditions where crystallization fouling is likely to occur under different operating conditions for three different desiccant solutions, namely magnesium chloride ($MgCl_2$), calcium chloride ($CaCl_2$) and lithium chloride (LiCl). The model is expanded to determine the fouling limits (which is attainment of saturation condition at the solution-membrane interface at the LAMEE outlet) in a counter-flow LAMEE. In addition, the moisture transfer flux decline due to crystallization fouling is analyzed for $MgCl_2$ at various locations along the LAMEE.

ACKNOWLEDGMENT

First and foremost, I would like to express my sincere gratitude to my supervisor, Professor Carey Simonson, for his invaluable comments, support, and guidance throughout this research project. Without his help, this research work could not be possible.

Special thanks go to my co-supervisor, Dr. Adesola Olufade, for his help and valuable feedback during my research.

I am also grateful to my Advisory Committee members, Prof. I. Oguocha and Prof. J. Bugg, for their valuable advice and assistance throughout this research.

I would also like to thank my research group members and postdoctoral fellows: Dr. Gurubalan Annadurai, Dr. Wahab O. Alabi, Mr. Hadi Ramin, Mr. Easwaran N. Krishnan, Mr. Bicheng Xing, Mr. Mehrdad Torabi, Mr. Teddy Okolo, and Mr. Mostafa Mostafavi Sani.

I gratefully acknowledge the financial support from the Saskatchewan Innovation and Opportunity Scholarship, Department of Mechanical Engineering at the University of Saskatchewan, and National Science and Engineering Research Council (NSERC) of Canada.

DEDICATION

I dedicate this thesis to my wife Ghazal and my family for their abiding love, encouragements and supports.

TABLE OF CONTENTS

Page

LIST OF TABLES

LIST OF FIGURES

NOMENCLATURE

Acronyms

HVAC	Heating, ventilation, and air-conditioning
LAMEE	Liquid-to-air membrane energy exchanger

Symbols

A	Clean area of the membrane, m^2
A_b	Blocked area of the membrane, m^2
a_w	Water activity in the solution
b	Solution molality, mol/kg
C^*	Dimensionless solution concentration
C_{DS}	Bulk concentration of desiccant solution, kg/m^3
$C_{DS,mem}$	Solution concentration on the membrane surface, kg/m^3
c_p	Specific heat capacity, J/(kg.K)
C_s	Saturation concentration, kg/m^3
Cr^*	Heat capacity rate ratio of the solution to the air
D_{AB}	Binary diffusion coefficient, m^2/s
D_h	Hydraulic diameter, m
h	Convective heat transfer coefficient, $W/(m^2.K)$
h_m	Convective mass transfer coefficient, $kg/(m^2.s)$
k	Thermal conductivity, W/(m.K)
K	Fouling rate constant, $m^6/(kg^2.s)$
K_s	Rate constant of surface crystallization, $m^4/(kg.s)$
L	Characteristic length, m
Le	Lewis number
m	Total mass deposited, kg
$\dot{m}_{Air}$	Air mass flow rate, kg/s
$\dot{m}_{DS}$	Desiccant solution mass flow rate, kg/s
$\dot{m}_d$	Deposition rate of crystals, kg/s
$\dot{m}_r$	Removal rate of crystals, kg/s

$\dot{m}^*$	Rate of change of the normalized moisture transfer flux ($\partial M^*/\partial t$), (1/s)
$\dot{m}_c''$	Moisture transfer flux through the clean membrane, kg/(m^2.s)
$\dot{m}_f''$	Moisture transfer flux through the fouled membrane, kg/(m^2.s)
M*	Normalized moisture transfer flux through the membrane
MW	Molecular weight of the solution, g/mol
NTU	Number of transfer units
NTU_m	Number of moisture transfer units
Nu	Nusselt number
p_v	Partial pressure of water vapor, Pa
$p_{v,sat}$	Water vapor saturation pressure, Pa
Pr	Prandtl number
R_{mem}	Vapor diffusion resistance of the membrane, s/m
R_w	Moisture flux ratio
Re	Reynolds number
RH_{air}	Air relative humidity, %
Sh	Sherwood number
T_{air}	Air stream temperature, °C
T_{DS}	Desiccant solution temperature, °C
U	Overall heat transfer coefficient, W/(m^2.K)
U_m	Overall mass transfer coefficient, kg/(m^2.s)
VDR	Vapor diffusion resistance, (s/m)
W_{air}	Air humidity ratio, kg_w/kg_{air}
W_{DS}	Equivalent humidity ratio of air in equilibrium with the desiccant solution, kg_w/kg_{air}
$W_{DS,mem}$	Humidity ratio of air in equilibrium with desiccant solution at the solution-membrane interface, kg_w/kg_{air}
ΔT_{lm}	Log mean temperature difference
ΔW_{lm}	Log mean humidity ratio difference

Greek symbols

β	Area of membrane occupied per unit mass, m^2/kg

δ	Membrane thickness, m
ρ	Density, kg/m^3

Subscripts

air	Air
DS	Desiccant solution
in	Inlet
out	Outlet
mem	Membrane
min	Minimum

CHAPTER 1

INTRODUCTION

1.1 Fouling of energy exchangers

Fouling is a widespread problem which plagues many industries including oil/gas refineries, desalination units, food/diary industries and power plants. It is the formation and buildup of any type of undesired material such as particulate matter, organic and inorganic compounds on a solid surface, which can be a metal plate or a membrane [1]. Membrane fouling occurs when particles or solutes are deposited onto the membrane surface or within the membrane pores [2]. Fouling happens according to different mechanisms depending on the operating conditions, impurities in the fluid, and type of working fluids. The common mechanisms of fouling include particulate, crystallization, biological, chemical reaction, and corrosion [1].

Fouling formation is a complex phenomenon in the design of exchangers for heat and/or mass transfer, and membrane-based separation processes due to a large number of variables (e.g. fluid velocity, temperature, surface material of construction, etc.) and their interactions [3]. For example, an increase in flow velocity can reduce blockage from crystallization fouling in tubes, but using stainless steel as the surface material of construction shows more susceptibility to fouling than other materials. Thus, monitoring the fouling behavior and exchanger performance is quite a challenging task. Numerous techniques have been developed to monitor fouling, however most of them are experimental. As a result, developing reliable models could facilitate the prediction of fouling especially for long-term periods.

There are several detrimental impacts of fouling on the operation of exchangers which include increased pressure drop, reduced effectiveness, deterioration of product quality, system downtime, and elevated costs of maintenance and cleaning processes [4]. The costs imposed by fouling of heat exchangers are estimated to be about 0.25% of gross domestic product of industrialized countries [5]. Moreover, as a rough estimate, heat exchangers fouling might be responsible for up to 2.5% of the worldwide CO_2 emissions [5]. Hence, developing predictive models, mitigation techniques, and cleaning strategies are necessary in addressing fouling.

1.1.1 Fouling in HVAC industry

Heating, ventilation, and air-conditioning (HVAC) systems are increasingly being used in residential, commercial, and industrial buildings. HVAC systems are responsible for nearly 50% of the energy consumption in buildings and around 10–20% of the total energy consumed in developed countries [6]. As a result, it is necessary to develop energy efficient HVAC systems.

A great number of studies have investigated the effect of fouling on the performance of heat exchangers in HVAC applications [7–12]. These studies include both air-side fouling and water-side fouling. Studies also found that fouling of heat exchangers in the HVAC industry can impose several economic and technical issues. Pak et al. [13] investigated the fouling of one-row HVAC condenser coils and found that the one-row coils lead to an increase in airside pressure drop up to 31% and a decrease in heat transfer rate up to 12%. The results of an experimental study showed that 50% blockage of the condenser due to fouling in a vapor compression refrigeration system leads to approximately 10% increase in compressor power consumption [14].

There are numerous studies on crystallization fouling in boilers, condensers, cooling towers, hot water heat exchangers, and other devices [13–20]. These studies focused on design parameters, fouling detection, fouling mitigation using equipment or structural modifications and/or inserts, inhibitors, etc.

Despite the large amount of research on crystallization fouling of heat exchangers in HVAC applications, there are limited studies on fouling of membrane-based energy exchangers. Furthermore, all of the studies on membrane fouling in HVAC systems are experimental studies which include fouling characterization in evaporative cooling systems [21,22], fouling detection and characterization in membrane energy exchangers [23–26], and fouling reversal in membrane energy exchangers [27]. There is limited research that has focused on modeling approaches that is useful for long-term operations. As a result, this thesis focuses on developing a model to study fouling in membrane energy exchangers under different operating conditions also for longer periods of operation.

1.2 Liquid-to-air membrane energy exchangers (LAMEEs)

Generally, there are two types of liquid desiccant energy exchangers; direct-contact and indirect-contact. In direct-contact exchangers, air passes over a surface that is wetted by a liquid desiccant

during which the liquid droplets might be entrained into air stream. The desiccant aerosols are corrosive to the air handling equipment and may be health hazards, which hinders the application of direct contact liquid desiccant energy exchangers. Recently, semi-permeable membranes have been investigated to separate air streams and desiccant streams in HVAC systems, and exchangers which use these membranes are referred to as liquid-to-air membrane energy exchangers (LAMEEs). Figure 1.1 shows a photo of two LAMEE prototypes and Figure 1.2 depicts a schematic of a counter-flow LAMEE. The membrane is only permeable to water vapor which allows simultaneous heat and mass transfer between the air and desiccant streams. LAMEEs work based on a vapor pressure difference across the membrane which is the driving potential for separation from the aqueous salt solution. For efficient performance of LAMEEs, the membrane needs to have low vapor diffusion resistance, high liquid penetration pressure, and high modulus of elasticity [28].

Extensive research has been done on LAMEEs from various perspectives including energy, environmental, and economical [28, 30–34]. The experimental results of Ref. [34] showed that the sensible and latent effectivenesses of a small-scale LAMEE can range from 75% to 120% and 70% to 90%, respectively, depending on the temperature and humidity ratio of the inlet air.

Figure 1.1. A photo of two LAMEE prototypes [29].

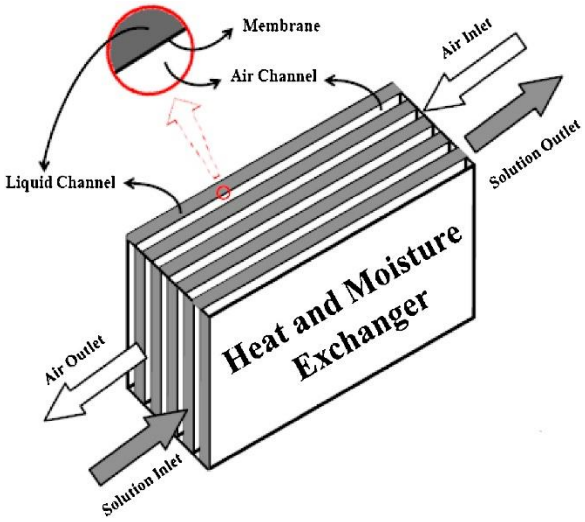

Figure 1.2. Schematic of a counter-flow LAMEE [28].

There are several benefits of LAMEEs that can be used as either active regenerators or dehumidifiers depending on whether the air is humidified or dehumidified, respectively [28]. LAMEEs can effectively remove gaseous pollutants such as CO, CO_2, NO_x, SO_x, and Formaldehyde from the supply air during the heat and mass transfer process since liquid desiccants are able to absorb these pollutants [30]. In terms of economy, LAMEEs can reduce the annual cooling energy consumption by about 50%, increase the annual heating energy consumption by about 140%, reduce the total energy consumption by 20%–60% and minimize CO_2 emissions by 20% compared to the conventional HVAC systems [31].

Beside the aforementioned benefits, there are some issues which may impact the LAMEE performance. One of the main issues is crystallization fouling of the membrane which will most likely occur at regeneration process (a process where moisture is removed from a diluted salt solution) due to the temperature elevation on the solution side. This research focuses on crystallization fouling due to reasons explained in the following section.

1.3 Crystallization fouling in LAMEEs

Crystallization fouling happens because of the precipitation of dissolved salts from an aqueous salt solution that accumulate on the membrane or other heat transfer surfaces. Supersaturation of the solution is the principal step in any crystallization process that may be the result of water evaporation, changes in temperature, addition of solute, or the mixing of solutions [35]. In some

conditions during the operation of a LAMEE, moisture transfers from the desiccant solution to the air, which dries the solution and may result in the solution attaining saturation conditions. Hence, there is a high chance of crystallization fouling in LAMEEs during regeneration, which can reduce the moisture transfer rate.

The high vapor pressure gradient through the membrane leads to greater moisture transfer rate and consequently high fouling rate in LAMEEs. Once this gradient field leads to supersaturation on the membrane, nucleation and growth of crystals occur within the membrane pores (internal fouling) or on the membrane surface (external fouling), as depicted in Figure 1.3. As water evaporates through the membrane in LAMEEs, the solution concentration on the membrane may achieve supersaturation which triggers crystal formation and growth. Figure 1.4 presents scanning electron microscopy images of a fresh membrane and a fouled membrane, extracted from Ref. [26]. As it can be observed, the crystal layer has covered the surface of the membrane which may block the active membrane pores for moisture transfer through the membrane.

Several factors might affect the rate of crystallization fouling in LAMEEs including the air and solution temperature, air moisture content, solution concentration, membrane properties, and flow conditions. Changing one or some of these factors may create a case where there is a high or low chance of crystallization fouling of the membrane.

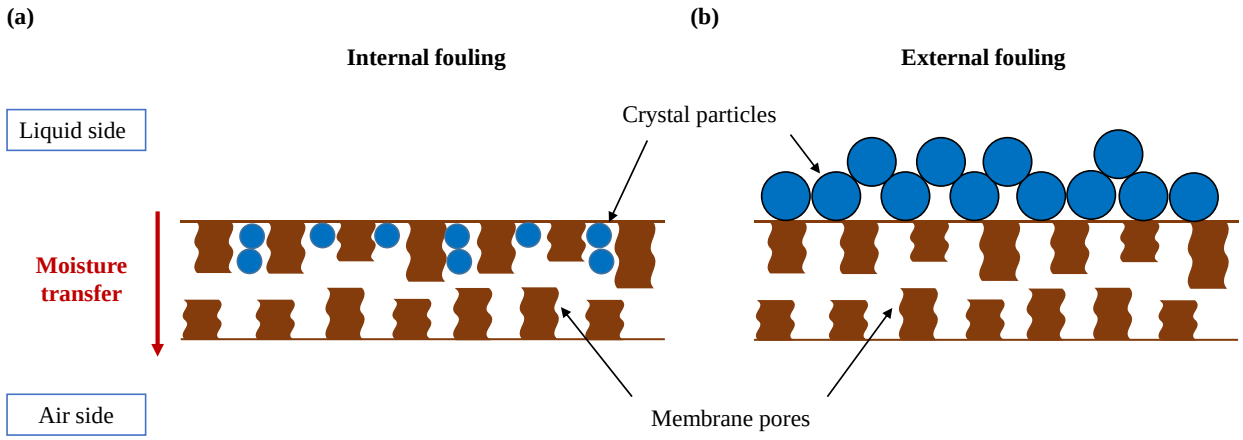

Figure 1.3. Schematic of fouling (a) within the membrane pores (internal fouling) and (b) on the membrane surface (external fouling).

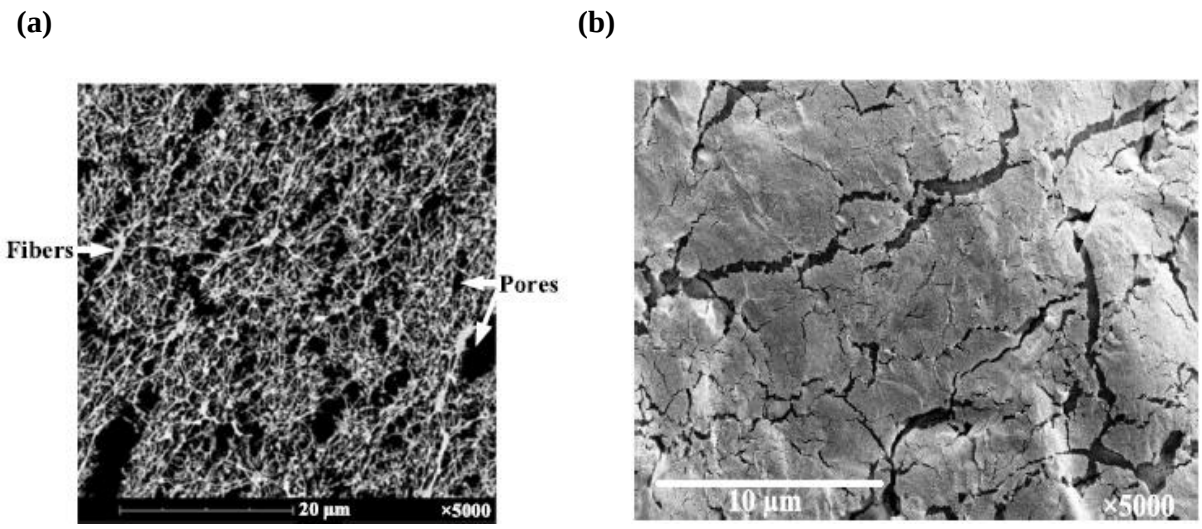

Figure 1.4. Comparison between a (a) fresh membrane and (b) fouled membrane with a solution concentration of 3% above saturation at air relative humidity of 10% [26].

Crystallization fouling in LAMEEs is a challenging problem and there are few studies on the topic, as mentioned in Section 1.1.1. Nonetheless, all of these studies are limited to detection, characterization and visualization of fouling through experimentation. Previous studies have discussed crystallization fouling in LAMEEs using fouling characterization by decrease in effective membrane porosity or decline in moisture transfer flux. Besides, crystallization fouling have been investigated by visualizing the membrane surface through scanning electron microscopy, digital microscopy, and X-ray diffraction. The fouling experiments may be done for a few operating and/or design conditions, short-term periods, and there could be quite high uncertainties in the results. Fouling experiments are often accelerated and unrealistic due to the slow mechanisms of fouling and may not capture certain elements of long-term fouling growth. Hence, there is a need for a model that can predict the fouling rate for long-term periods and for different design/operating conditions. This research fills the gap in the literature by developing a model for a LAMEE which predicts the fouling rate, moisture transfer flux decline due to fouling, and the operating/design conditions where fouling is likely to occur.

1.4 Thesis objectives

As noted in the previous sections, there is scarcity of research on predicting fouling in LAMEEs for HVAC applications. For LAMEEs which are subject to crystallization fouling on the liquid side, it is important to monitor the trend of moisture transfer rate and determine the cleaning

frequency. Moreover, as mentioned above, previous work on LAMEE fouling has focused only on experimental methods and there is a lack of research on modelling. Hence, the main goal of this research is to model fouling in LAMEEs. The specific objectives of this thesis are to:

1. Develop and validate a predictive model for determining the moisture transfer rate in LAMEEs due to crystallization fouling, and
2. Quantify the impact of design and operating conditions on crystallization fouling in LAMEEs.

1.5 Thesis structure

This thesis is a manuscript-style thesis which is based on the submitted manuscripts. The thesis contains four chapters where Chapter 1 gives an introduction of the thesis. In Chapter 2, a semi-empirical model is developed for predicting the fouling rate of membranes in LAMEEs and the decline in moisture transfer rate is estimated. Chapter 3 focuses on developing a crystallization fouling limit model for a range of operating and design conditions using a modified version of the model in Chapter 2.

1.6 List of publications

The following papers constitute Chapters 2 and 3 in this thesis:

Chapter 2: A. Razmavar, G. Annadurai, A. Olufade, C.J. Simonson, 2021, A model for predicting the effect of crystallization fouling on moisture transfer in membrane energy exchangers, Submitted to International Journal of Heat and Mass Transfer.

Chapter 3: A. Razmavar, G. Annadurai, A. Olufade, C.J. Simonson, 2021, A theoretical study on crystallization fouling limits in liquid-to-air membrane energy exchangers, Submitted to ASME Journal of Heat Transfer.

CHAPTER 2

DEVELOPMENT OF A PREDICTIVE MODEL FOR CRYSTALLIZATION FOULING

2.1 Overview

The primary goal of this chapter is to develop a predictive model for determining the fouling rate and moisture transfer flux decline due to fouling in LAMEEs. The model is validated with experimental data from the literature and then is used to predict the effect of different operating and design parameters on the fouling rate. A brief description of the fouling test facility used to validate the model is also presented in this chapter. The modeling and experimental results show that over time, the formation and growth of crystals covers an area of the membrane surface which consequently reduces the moisture transfer through the membrane.

This chapter includes a manuscript submitted to the International Journal of Heat and Mass Transfer. The four authors of this paper are Alireza Razmavar (M.Sc. student) who developed the model and prepared the original manuscript, Gurubalan Annadurai (Postdoctoral Fellow) who reviewed the manuscript, Adesola Olufade (Co-supervisor) who measured the experimental data and reviewed the manuscript, and Professor Carey Simonson (Supervisor) who critically reviewed the manuscript and supervised this study.

A model for predicting the effect of crystallization fouling on moisture transfer in membrane energy exchangers

Alireza Razmavar, Gurubalan Annadurai, Adesola Olufade, Carey J. Simonson

2.2 Abstract

Crystallization fouling is an important phenomenon that impacts the design and operation of membrane-based separation processes. Recently, membranes have been applied to separate aqueous salt solutions and air streams for moisture control in buildings using liquid-to-air membrane energy exchangers (LAMEEs). LAMEEs are efficient energy exchangers that use a semi-permeable hydrophobic membrane to separate air and aqueous salt solutions, while allowing simultaneous heat and moisture exchange between the fluids. However, in some design and operating conditions, crystallization fouling occurs which hinders the performance of LAMEEs. The main objective of this chapter is to develop a model which predicts the fouling rate for membranes in LAMEEs. The semi-empirical model estimates the decline in moisture transfer rate by taking into account the surface blockage of the membrane due to crystallization fouling. The model is validated with experimental data available in the literature. The model can then be used to predict the theoretical crystallization fouling limits and the effect of design and operational parameters on fouling rates. For example, the initial fouling rate is four times higher for a supersaturated solution (3% above saturation) than for a saturated solution.

2.3 Introduction

Fouling is defined as the deposition of unwanted materials on a surface [1]. Fouling is a primary challenge in membrane separation processes since fouling can cover the surface of a membrane (external fouling) or fill the pores within the membrane (internal fouling) [2]. Fouling can cause adverse impacts on the performance of heat exchangers and membrane-based separation processes leading to various problems such as additional maintenance costs, reduced lifespan of the equipment, and production loss [4,17,36,37]. It has been estimated that the cost of heat exchangers fouling in most industrialized countries could be up to 0.25% of the gross domestic product [5]. The amount is about US$ 53 billion, US$ 39 billion, and US$ 4 billion for USA, European Union, and Canada, respectively, in 2019 using the World Bank Group data [38–40].

As with all membrane systems, an important issue for liquid-to-air membrane energy exchangers (LAMEEs) is crystallization fouling of the membrane which can remarkably reduce the moisture transfer rate. LAMEEs have recently been used in heating, ventilation, and air-conditioning (HVAC) applications which incorporate a micro-porous hydrophobic membrane to simultaneously transfer heat and moisture between an air stream and a liquid desiccant solution [30]. The liquid desiccants used in LAMEEs are aqueous salt solutions such as magnesium chloride ($MgCl_2$), calcium chloride ($CaCl_2$), lithium chloride (LiCl), and lithium bromide (LiBr) [41]. LAMEEs are able to operate more economically and more efficiently than traditional HVAC systems. LAMEEs have the potential to reduce the energy consumption of HVAC systems by 20%–60% and to reduce CO_2 emissions by 20% [30,31].

Despite numerous research on fouling of HVAC systems [19,42–46], only a few studies have been done on crystallization fouling in LAMEEs, which is a research gap that has been identified in recent review papers [30,47]. Some research on ionic liquids has also been conducted to avoid the crystallization problem, but the added cost may be prohibitive [48]. This chapter will focus on the modeling of crystallization fouling in LAMEEs because previous works have mainly focused on experimental studies described in the next section. An important limitation of experiments is that the test conditions are extreme (not realistic or practical) in order to accelerate fouling. An advantage of a model would be the ability to use realistic conditions to simulate prolonged fouling in LAMEEs.

2.3.1 Experimental studies of fouling in LAMEEs

Charles and Johnson [21] performed an experimental study to characterize fouling in hollow fiber type LAMEE for an evaporative cooling process with potable tap water. They used scanning electron microscopy to visualize membrane deterioration due to fouling. In an experimental study, Crawford and da Silva [22] investigated the performance of a membrane evaporative cooling system under fouling conditions. The study used a high quality imaging to characterize the fouling layer and monitor the change in moisture transfer flux. According to these two studies, crystallization fouling could lead to nearly 90% decrease in moisture transfer rate through the membrane.

In research works of Olufade and Simonson [23–25], the onset of crystallization fouling was detected three to eight times earlier using digital microscopy as opposed to monitoring the changes in moisture flux. Olufade and Simonson [26] also implemented scanning electron microscopy, optical microscopy, and X-ray diffraction to characterize crystal particles on the membrane surface of a LAMEE. Although they could not confirm internal fouling, their observations demonstrated that external fouling is the prevailing mechanism.

2.3.2 Modeling of fouling in membrane distillation and reverse osmosis

The heat and moisture transfer processes in membrane distillation and LAMEEs are very similar, with vapor pressure gradient being the driving potential for water vapor transfer in both LAMEEs and membrane distillation. Although many studies exist on membrane distillation fouling [49–52], there are limited studies focused specifically on modeling of crystallization fouling [53–56]. Warsinger et al. [53] used classical nucleation theory to predict the onset of fouling and developed regime maps that identified the operating conditions under which fouling would not occur. However, the impact of fouling on water vapor flux was not discussed. There are two theoretical studies which considered flux decline in membrane distillation due to fouling [54,56]. In the first one, flux decline was attributed to the intermediate pore blocking (i.e., blockage of a portion of the pores by a number of particles while other particles deposit on a pre-deposited layer) as well as cake formation on the membrane surface [54]. The second study implemented the surface blockage method to determine the flux decline which is due to the crystals growing laterally on the membrane surface [56].

Flux decline due to crystallization fouling has also been a problematic issue in reverse osmosis processes. In former studies of [57–59], the surface blockage method was developed for reverse osmosis systems to investigate the rate of flux decline. In this chapter, the surface blockage method will be applied to LAMEEs to model the moisture transfer flux reduction due to crystallization fouling. It should be noted that the model does not distinguish between pore and surface blockage.

2.3.3 Focus and objectives

Considering the literature related to fouling highlighted above, crystallization fouling of LAMEEs has been studied from an experimental perspective. The experimental results agree that fouling would bring about the reduction of moisture transfer flux through the membrane, and hence

deteriorates the LAMEE performance. Nonetheless, there is limited research on determining the variations of moisture transfer flux due to crystallization fouling through modeling. Thus, this chapter aims at filling this research gap by developing a semi-empirical model which can predict the trend of moisture transfer flux and fouling rate in a LAMEE during crystallization fouling.

After the model is validated with the experimental data from the literature [23–25,27], the model will be used to predict the time when moisture transfer flux declines to a certain value due to the fouling. A valuable outcome of the model is that it can estimate the time to clean or replace the membrane which can help the designers oversee the membrane performance. Moreover, the crystallization fouling limits are identified for a range of design and operating conditions.

2.4 Model description

2.4.1 Theoretical background of crystallization fouling

Crystallization fouling is referred to as the precipitation of ions from an aqueous salt solution on heat transfer or membrane surfaces. Three basic stages in crystallization fouling are: (1) attainment of supersaturation, (2) crystal nucleation, and (3) crystal growth [60]. The first requirement for any crystallization process is the supersaturation of an aqueous salt solution in which the solution concentration is greater than the saturation concentration at a given temperature [60]. An aqueous salt solution can become supersaturated through four different ways as follows: i) when normal solubility salts (their solubility increases by increasing temperature, e.g. NaCl and $MgCl_2$) are cooled below their solubility temperature, ii) when inverse solubility salts such as $CaSO_4$ and $CaCO_3$ are heated above their solubility temperature, iii) when the solution is evaporated until it reaches to its saturation limit, and iv) when the solution is mixed with other solutions [60,61].

Upon attaining the supersaturation, it is likely that the nuclei are formed and crystal nucleation happens due to the presence of impurities in the bulk solution or imperfections on the surface [60]. There are two possible nucleation processes that can occur, i.e. spontaneous and artificial [61]. Over time, the crystals formed during the nucleation process grow until their size is detectable. This process is considered as crystal growth which can occur through two steps. In the first step, ions are transported from the bulk toward the liquid-crystal interface and then in the second step, ions at the surface are integrated into a crystal lattice [61,62].

There are two pathways through which the crystallization process occurs; bulk crystallization and surface crystallization. In the former, the formation of crystal particles takes place in the bulk solution and particles are then transported to the surface, while in the latter both the nucleation and crystal growth occurs on the surface [49].

2.4.2 Fouling model

A schematic diagram of moisture transfer through a hydrophobic membrane in a LAMEE is depicted in Figure 2.1. The properties of the membranes used in this study are listed in Table 2.1. As shown in Figure 2.1, dry air flows beneath the membrane and a desiccant solution ($MgCl_2$) exists on top of the membrane. Moisture transfers from the desiccant solution to the air stream, thus the dry air is humidified.

As depicted in Figure 2.1, due to the evaporation of water vapor from the desiccant solution to the air and moisture permeation through the membrane, the concentration at solution-membrane interface increases until it may attain supersaturation. As mentioned before, supersaturation is a prerequisite for nucleation and crystal formation on the membrane surface. Once nucleation occurs, crystal particles grow on the membrane surface via bulk and/or surface crystallization [57]. Generally, bulk crystallization is more prevalent at high supersaturation level [62]. Since in the experiments, the solution is either saturated or slightly above saturation (only 3%), it is assumed that there is no bulk crystallization in this study.

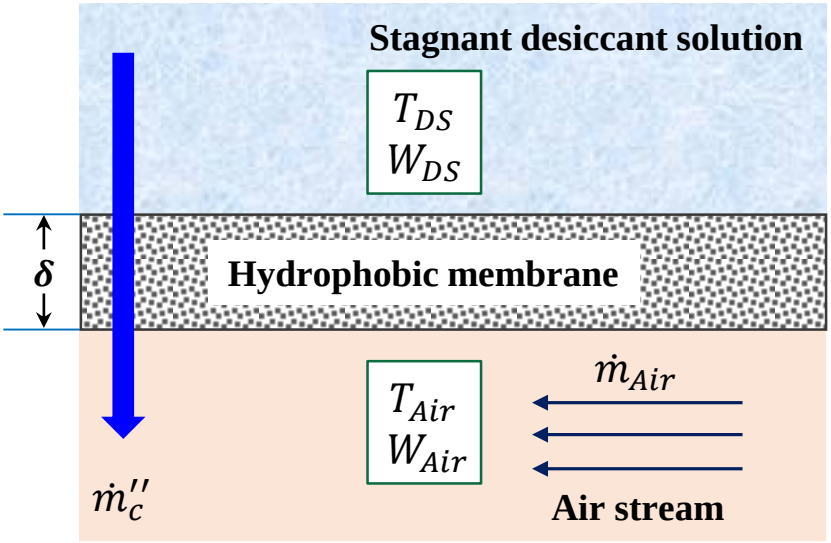

Figure 2.1. Schematic of moisture transfer between the desiccant solution and air stream through the membrane.

Table 2.1. Specifications of the membranes used in this study.

Parameter	**Membrane A** [24]	**Membrane B** [24]
Material	ePTFE laminates	ePTFE surface and PP support
VDR (s/m)	97	23
Porosity (%)	85	-
Pore size (μm)	0.3	0.2
Thickness (mm)	0.54	0.13

Note: ePTFE: Expanded Polytetrafluoroethylene; PP = Polypropylene.

There are two fundamental mechanisms that can lead to flux decline through the membrane. The first mechanism is cake formation which is caused by bulk crystallization. The second one is surface blockage which is the consequence of surface crystallization [58,63]. In the cake formation mechanism, the flux decline occurs because of the deposition of crystal particles formed in the bulk phase, as depicted in Figure 2.2(a). In the surface blockage mechanism, the flux decline is related to the coverage of the membrane pores by particles growing laterally on the surface, as shown in Figure 2.2(b). In this case, a portion of the membrane surface is covered by crystals, while some areas of the membrane being free of deposit. A larger area of the membrane is covered as more crystal particles grow laterally on the membrane surface. As mentioned before, since the solution in this study is not highly supersaturated, it is assumed that bulk crystallization does not occur. Therefore, it is assumed that surface crystallization occurs on the membrane leading to an increase in the surface blockage.

A widely used model for the fouling process was first proposed by Kern and Seaton [64]. In this model, the net fouling rate (dm/dt) is equal to the difference between the deposition rate ($\dot{m}_d$) and the removal rate ($\dot{m}_r$) represented by:

$$\frac{\mathrm{dm}}{\mathrm{dt}} = \dot{m}_d - \dot{m}_r \tag{2.1}$$

In Eq. (2.1), the deposition rate is initiated by the driving forces that transport the particles to the surface, while the removal rate is related to the shear stress due to the fluid flow velocity [44,65]. Since the solution in this study is stagnant and there would be no shear stress, the removal rate is

believed to be small and be neglected. Therefore, the net fouling rate would equal to the deposition rate:

$$\frac{dm}{dt} = \dot{m}_d \tag{2.2}$$

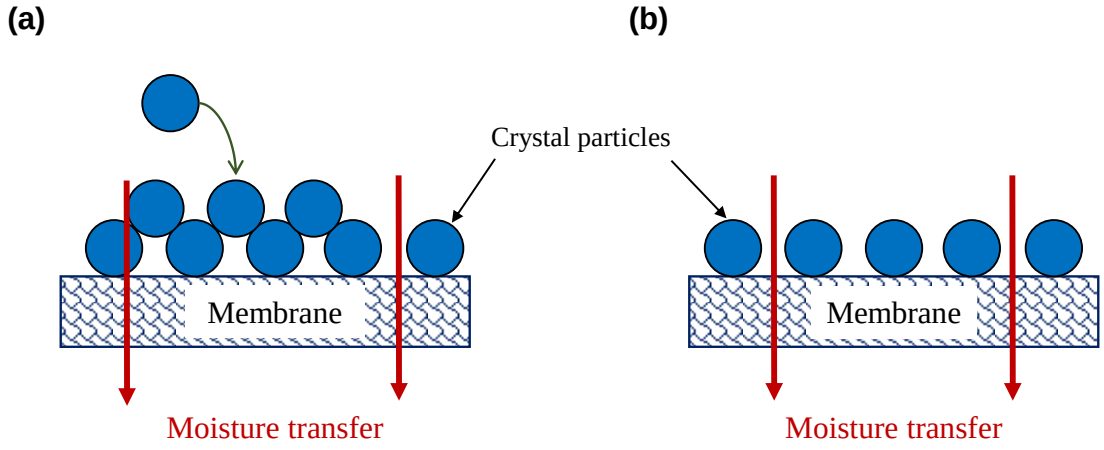

Figure 2.2. A sketch showing the flux decline due to (a) cake formation and (b) surface blockage.

In a model developed in [58,66], the two mechanisms of bulk and surface crystallization were taken into account to determine the flux decline due to fouling in a reverse osmosis system. The authors used the following equation to determine the rate of surface crystallization on the membrane [58,66]:

$$\dot{m}_d = K_s(A - A_b)(C_{DS,mem} - C_s)^n = K_s A\left(1 - \frac{A_b}{A}\right)(C_{DS,mem} - C_s)^n \tag{2.3}$$

where K_s is the rate constant of surface crystallization, A is the membrane area, A_b is the blocked area of the membrane surface, $C_{DS,mem}$ is the solution concentration on the membrane surface, C_s is the saturation concentration, and n is the order of reaction rate. According to the literature [67,68], the order of reaction corresponds to the number of ions participating in the formation of crystal lattice. Therefore, based on the aqueous salt solution used in this chapter, which consists of Mg^{2+}, the reaction would be second order. It should be noted that the procedure to obtain $C_{DS,mem}$ will be explained in section 2.4.3.

The area of the membrane blocked by the crystal particles (A_b) could then be expressed as [58,66]:

$$A_b = \beta m \tag{2.4}$$

where β is the area occupied per unit mass.

In the surface blockage model, the portion of membrane area covered by crystal particles is not permeable to water vapor transfer, thus, moisture transfer is only through the uncovered area [54,58,66]. However, in reality, the crystal particles forming/growing on the membrane surface would form a porous structure which would impede moisture transfer but not stop it entirely. Nevertheless, in this study, it is assumed that reduced moisture transfer flux due to crystallization fouling ($\dot{m}_f''$) can be approximated by moisture transfer flux without fouling ($\dot{m}_c''$) through the uncovered membrane area ($A - A_b$) which can be written as [54,66]:

$$\dot{m}_f'' = \dot{m}_c'' \frac{A - A_b}{A} \tag{2.5}$$

By combining and solving Eq. (2.2) to (2.5), the normalized moisture transfer flux (M*) through the membrane can be given by:

$$M^* = \frac{\dot{m}_f''}{\dot{m}_c''} = 1 - \left(1 - \exp\left[-K\left(C_{DS,mem} - C_s\right)^2 t\right]\right) \tag{2.6}$$

where $K = K_s\beta$ is a fouling rate constant that can be determined from the experimental data. The rate of change of the normalized moisture transfer flux ($\dot{m}^*$) is also important because it represents the fouling rate (or blockage rate) and is given by:

$$\dot{m}^* = \frac{\partial A_b}{\partial t} = -\frac{\partial M^*}{\partial t} \tag{2.7}$$

2.4.3 Concentration at solution-membrane interface

The concentration at the solution-membrane interface is calculated using the mass transfer balance in a control volume on the membrane surface [69]. Eq. (2.8) is used to calculate moisture transfer flux ($\dot{m}_c''$), depicted schematically in Figure 2.1, through the membrane due to the humidity ratio (W) difference [69]:

$$\dot{m}_c'' = U_m(W_{DS,mem} - W_{Air}) = h_{m,DS}(C_{DS,mem} - C_{DS}) \tag{2.8}$$

where U_m is the overall mass transfer coefficient, C is the concentration, h_m is the mass transfer coefficient, and the subscripts DS represents desiccant solution, DS, mem represents desiccant solution on the membrane, and Air represents air.

$W_{DS,mem}$ in Eq. (2.8) is the humidity ratio in equilibrium with the desiccant solution at the solution-membrane interface which is a function of solution temperature and desiccant solution concentration at the membrane surface. Since in this study, the LAMEE is operated at isothermal conditions, the humidity ratio is only a function of desiccant solution concentration. $W_{DS,mem}$ can be written as [70]:

$$W_{DS,mem} = 0.62198 \frac{p_v}{P - p_v} \tag{2.9}$$

where P is the total pressure and p_v is the water vapor partial pressure at the solution-membrane interface calculated by [71]:

$$p_v = a_w p_{v,sat} \tag{2.10}$$

where a_w is the water activity in the $MgCl_2$ solution that can be obtained from the following correlation based on the data of Ref. [72]:

$$a_w = 0.00018b^4 + 0.00021b^3 - 0.0206b^2 - 0.0375b + 0.9996 \tag{2.11}$$

where b is the molality of the desiccant solution. $p_{v,sat}$ in Eq. (2.10) represents the pure water saturation pressure given by the Antoine equation in which $p_{v,sat}$ is calculated in Pa based on temperature T in Kelvin [71]:

$$p_{v,sat} = \exp\left(23.5377 - \frac{4016.3632}{T - 38.6339}\right) \tag{2.12}$$

U_m in Eq. (2.8) is expressed as:

$$U_m = \left(\frac{1}{h_{m,Air}} + \frac{R_{mem}}{\rho_{Air}}\right)^{-1} \tag{2.13}$$

where $h_{m,Air}$ is the convective mass transfer coefficient of air, R_{mem} is the vapor diffusion resistance (VDR) of the membrane and ρ is density.

$h_{m,DS}$ in Eq. (2.8) is computed from the definition of Sherwood number (Sh) as follows:

$$h_{m,DS} = \frac{ShD_{AB}}{D_h} \tag{2.14}$$

where D_h is the hydraulic diameter and D_{AB} is the diffusion coefficient of the desiccant solution. Since the desiccant solution is stagnant in the experiments, the value of Sherwood number is one. The following equation can be used in order to find the diffusion coefficient of $MgCl_2$ solution at 25°C [73]:

$$D_{AB} = 10^{-11} \times (103 + 3.84b + 6.4b^2 - 3.86b^3 + 0.4b^4) \tag{2.15}$$

The Chilton-Colburn analogy is used to determine the convective mass transfer coefficient of air ($h_{m,air}$) defined in Eq. (2.13). This analogy is expressed as [74]:

$$\frac{h}{h_{m,Air}} = c_p Le^{2/3} \tag{2.16}$$

where c_p is the specific heat capacity of air, Le is the Lewis number, and h is the heat transfer coefficient of air which can be obtained from the definition of Nusselt number (Nu):

$$h = \frac{Nuk}{D_h} \tag{2.17}$$

where k is the thermal conductivity of air. Since the air stream passes through a circular pipe and the flow is fully developed laminar, Hausen's correlation is usually recommended to determine the Nusselt number [75]:

$$Nu = 3.658 + \frac{0.085[RePr(D_h/L)]}{1 + 0.047[RePr(D_h/L)]^{0.67}} \tag{2.18}$$

where Re is the Reynolds number, Pr is the Prandtl number, and L is the pipe length.

Iterating Eq. (2.8) and employing Eq. (2.9) to (2.18) gives the desiccant concentration at the solution-membrane interface ($C_{DS,mem}$). The flowchart for calculating the normalized moisture transfer flux is depicted in Figure 2.3.

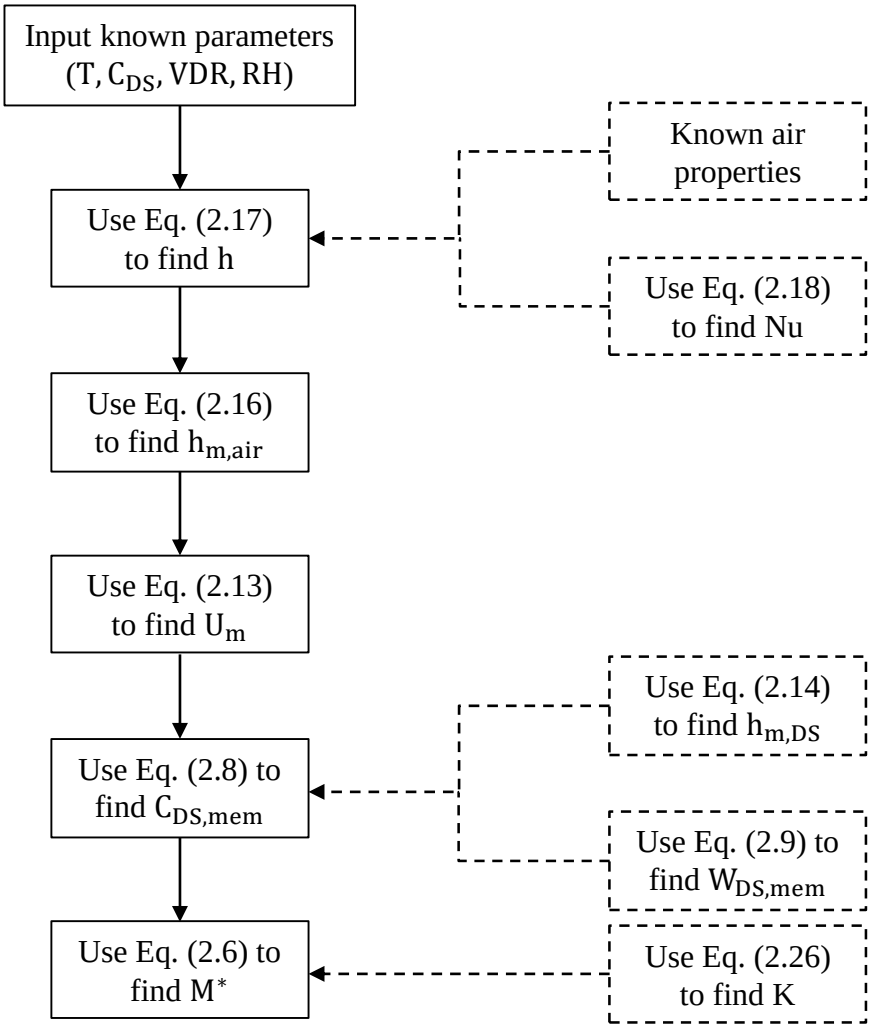

Figure 2.3. Flowchart for calculating the normalized moisture transfer flux.

2.5 Experiments

A test facility is used to investigate the effect of crystallization fouling on moisture transfer flux through the membrane. A brief description of the experimental test facility is given in this section, since it has been explained in detail in Ref. [23]. Figure 2.4 presents a schematic diagram of the test facility consisting of a cross-section side view of the LAMEE (Figure 2.4b) and the arrangement of the perforated holes in the inner pipe of the LAMEE (Figure 2.4c).

The LAMEE is a double-pipe heat exchanger which is made up of the inner pipe and outer pipe. Air passes through the inner pipe while the stagnant desiccant solution is filled in the outer pipe. The membrane is placed on the holes providing the areas of active moisture transfer between the desiccant solution and air stream.

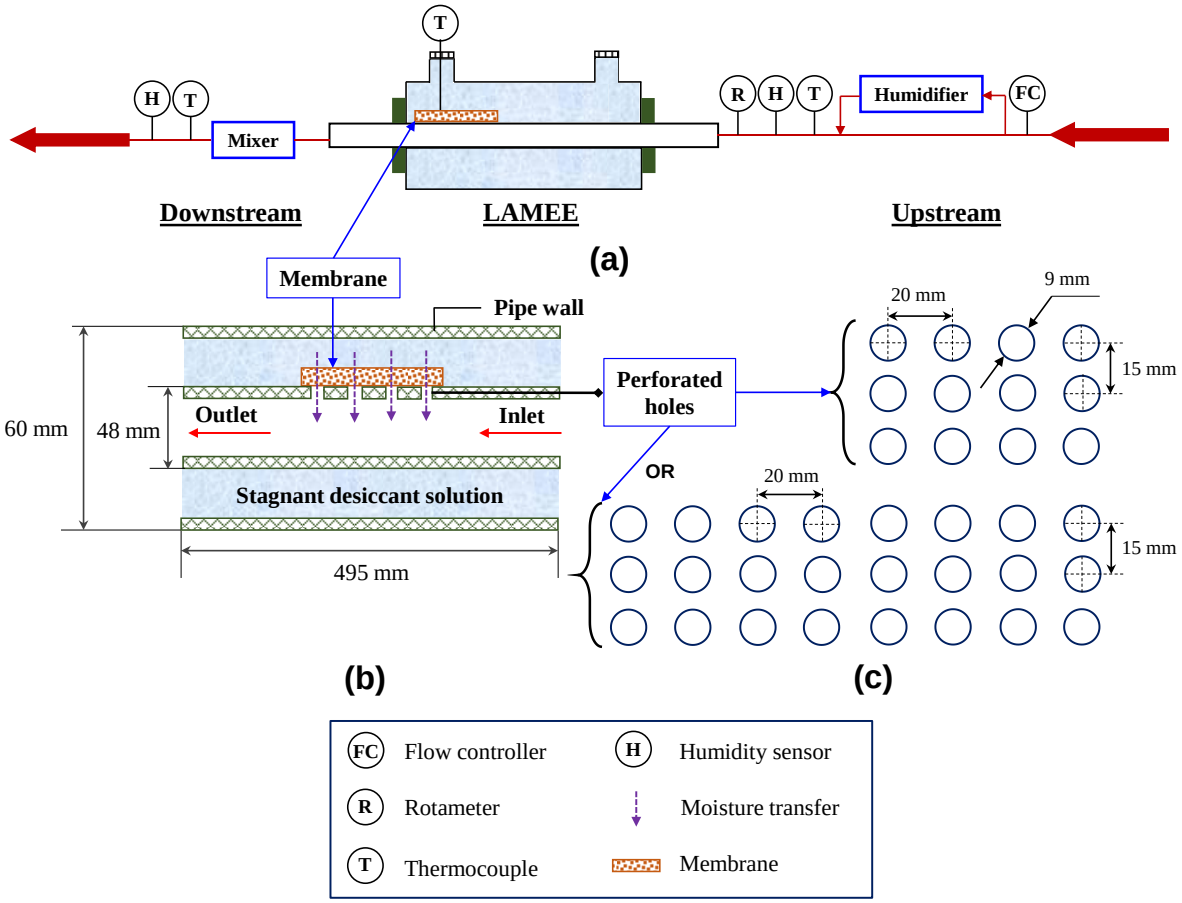

Figure 2.4. A sketch of (a) the test facility, (b) cross-section side view of the LAMEE and (c) top view of the arrangement of perforated holes in the inner pipe of the LAMEE.

Dry air at room temperature (~22–24°C) is supplied to the upstream section of the LAMEE, as depicted in Figure 2.4(a). The humidity of the air is then adjusted using a humidifier. The flow rate of the air is controlled by a flow controller before the humidifier and a rotameter after the humidifier. In the downstream of the test section, a mixer is used to obtain uniform properties of air. The air mass flow rate ($\dot{m}_{Air}$) used in the experiments is 1.4×10^{-5} kg/s.

The tests were conducted at air relative humidity (RH_{air}) of 10% and 20% for two solution concentrations, i.e. C* ~ 1.0 (saturated) and C* ~ 1.03 (supersaturated), where C* is the dimensionless solution concentration defined as:

$$C^* = \frac{C_{DS}}{C_s} \tag{2.19}$$

The following equation is applied to calculate the moisture transfer flux through the membrane using the measured humidity ratio at pipe inlet ($W_{Air,in}$) and pipe outlet ($W_{Air,out}$) [23]:

$$\dot{m}_f'' = \frac{\dot{m}_{Air}(W_{Air,out} - W_{Air,in})}{A} \quad (2.20)$$

In order to normalize the moisture transfer flux, the following relation is implemented:

$$M^* = \frac{\dot{m}_f''}{\dot{m}_{c,o}''} \quad (2.21)$$

where $\dot{m}_{c,o}''$ is the moisture transfer flux at the start of steady state during a test. The time where the boundary conditions of desiccant solution and air reaches to equilibrium is expressed as the steady state period. It should be noted that the steady state period is with respect to the boundary conditions for data analysis not fouling. Detailed explanations of determining the start of steady state can be found in Ref. [23].

2.5.1 Experimental uncertainty

The uncertainties in experimental parameters are calculated from the uncertainties of measurements. The total uncertainty (U) is determined from the random (P) and systematic (B) uncertainties for a 95% confidence interval which is given by the following equation as per ASME PTC Standard 19.1 [76]:

$$U = \sqrt{P^2 + B^2} \quad (2.22)$$

The random uncertainty is determined by:

$$P = \frac{t'SD}{\sqrt{N}} \quad (2.23)$$

where SD is the standard deviation of all measurements, N is the number of measurements, and t' is the Student's t-factor at 95% confidence interval (which is nearly 2 for $N \geq 30$). The systematic uncertainty includes errors in calibration, data acquisition, and data reduction.

The temperature and relative humidity of air at the inlet and outlet of the LAMEE test section is measured using T-type thermocouples and Honeywell HIH humidity sensors, respectively. The thermocouples and humidity sensors are calibrated before the experiments. The systematic uncertainty in thermocouples and humidity sensors are ±0.1°C and ±0.5%, respectively. The total uncertainties for the thermocouples and humidity sensors are equal to ±0.2°C and ±1%,

respectively. The total uncertainties of the flow controllers and rotameters are ±1% and ±0.001 L/s, respectively. Table 2.2 presents the uncertainties in the normalized moisture transfer flux at various operating conditions.

Table 2.2. Calculated uncertainty values for normalized moisture transfer flux.

Operating condition	P	B	U
RH_{air} = 10%, C* = 1.0	4%	37–42%	37–42%
RH_{air} = 10%, C* = 1.03	4%	32–42%	32–42%
RH_{air} = 20%, C* = 1.03	2%	80 –86%	80 –86%

2.5.2 Mass and energy balances

Mass and energy balances are performed to ensure that mass and energy conservations are within the uncertainty limits of the experimental tests. The mass balance and energy balance are used to determine the difference between mass/energy gained by the air stream and mass/energy lost by the desiccant solution. Detailed explanations of mass and energy balances can be found in Ref. [23].

Mass gained by the air is measured by calculating the quantity of water evaporated to the air from the solution. Mass lost by the solution is measured by calculating the difference in mass of the LAMEE before and after the tests. It should be noted that the uncertainty in mass measurement is ±1.1 g. The energy balances for the air and solution are also verified for the experiments. The results, elaborated in Ref. [23], show that mass and energy balances between the air and desiccant solution lie within ±20% demonstrating that the moisture and energy flows are correctly measured.

2.6 Results and discussion

2.6.1 Determination of the fouling rate constant (K)

In order to determine the fouling rate constant (K), non-linear regression is performed using the experimental data of M^* and t as follows:

$$1 - \mathrm{M}^* = (1 - \exp[-\mathrm{K}\left(\mathrm{C}_{\mathrm{DS,mem}} - \mathrm{C}_{\mathrm{s}}\right)^2 \mathrm{t}] \quad (2.24)$$

Since $\mathrm{C}_{\mathrm{DS,mem}}$ is a constant known for every test condition and can be calculated using the equations described in section 2.4.3, the fouling rate constant is determined by curve fitting of 1-

M* versus time using the experimental data of Ref. [23–25,27]. Figure 2.5 shows the curve fitting for two test conditions mentioned in Table 2.3. Each curve fitting for tests A-D specified in Table 2.3 gives a unique value of $K(C_{DS,mem} - C_s)^2$ and K is found by calculating $C_{DS,mem}$ for every test condition. To find a correlation for K, it can be expressed as a function of supersaturation degree on the membrane surface (S_{mem}) which is defined as:

$$S_{mem} = \frac{C_{DS,mem}}{C_s} \tag{2.25}$$

Since the initial particles forming on the membrane surface are the nucleation sites that induce the deposit formation by crystal growth [59], the number of nucleation sites that are activated depends on S_{mem}. Therefore, by increasing the supersaturation degree, number of nucleation sites increases leading to an increase in β and consequently in K. All four calculated K values based on tests A-D are plotted versus S_{mem}, as shown in Figure 2.6, to get a correlation for K given by this equation:

$$K = 5 \times 10^{-10} {S_{mem}}^{41.7} \tag{2.26}$$

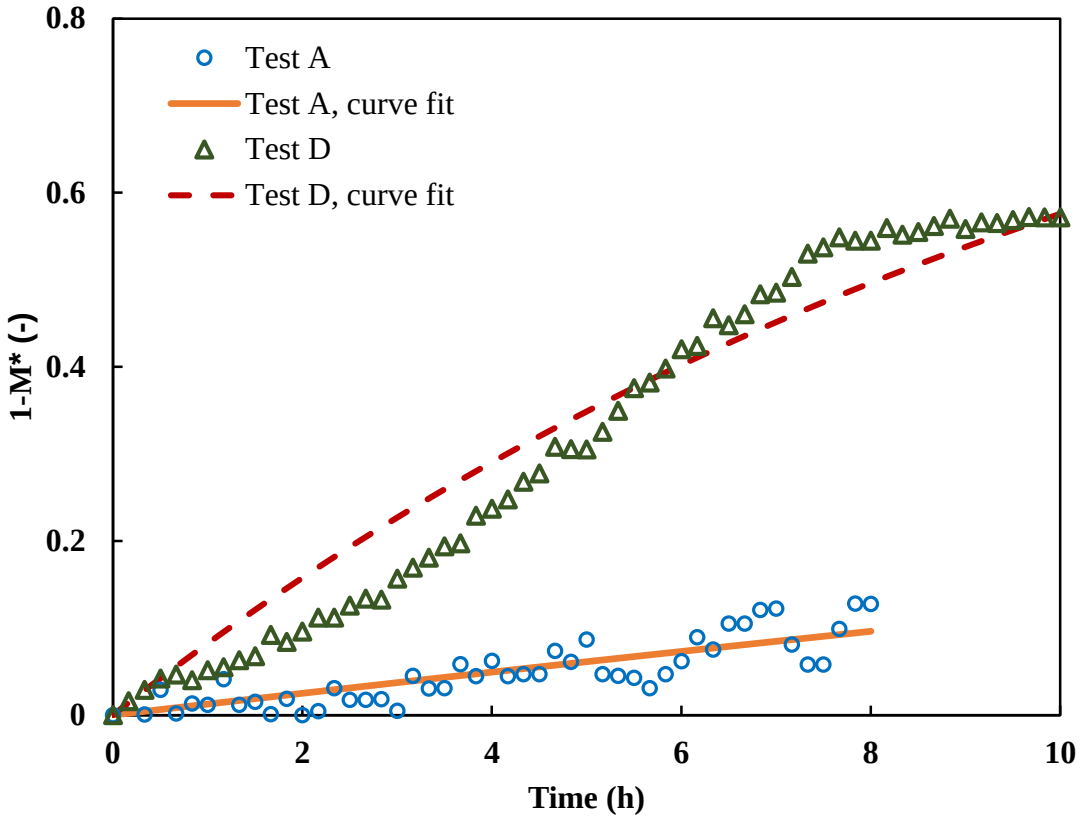

Figure 2.5. Curve fitting for tests A and D specified in Table 2.3.

Table 2.3. Experimental conditions used for curve fitting and model validation.

Function	Test	Temperature (°C)	RH_{air} (%)	C*	Membrane, VDR (s/m)	Testing time (h)	Ref.
Experimental data used for curve fitting	A	24	20	1.03	A, 97	8	[23]
	B	22	10	1.0	A, 97	10	[27]
	C	24	10	1.0	A, 97	10	[23]
	D	23	10	1.03	A, 97	10	[23–25]
Experimental data used for model validation	E	22	10	1.03	B, 23	10	[24]
	F	24	20	1.03	B, 23	8	[24]
	G	22	10	1.03	A, 97	20	[27]

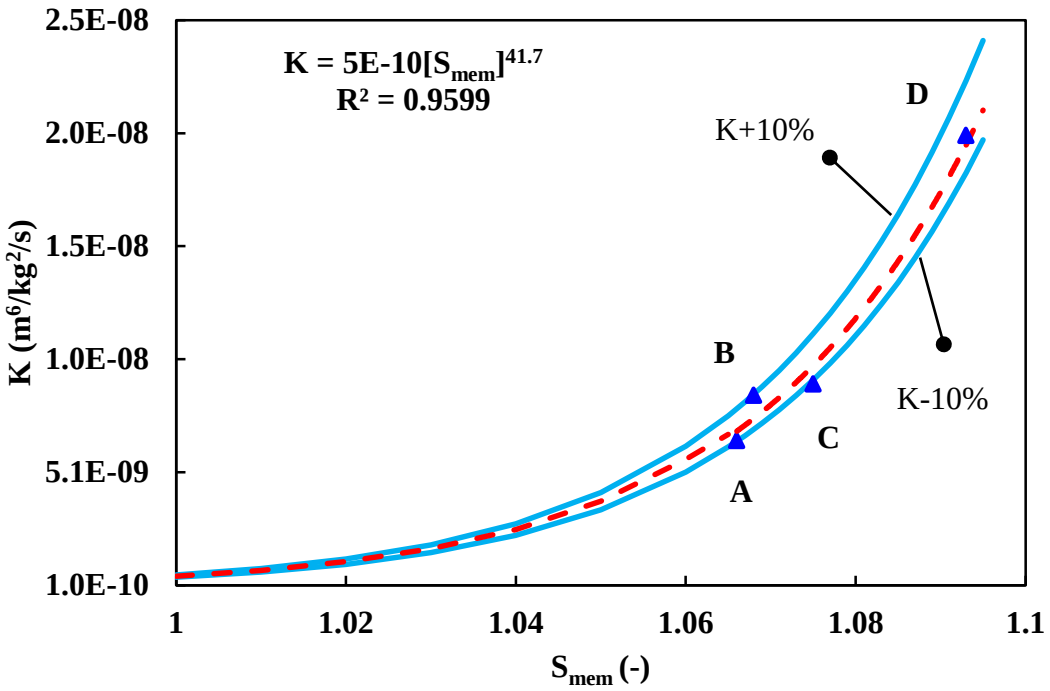

Figure 2.6. The fouling rate constant (K) as a function of supersaturation degree on the membrane surface (S_{mem}). Note: The operating conditions for tests A–D are given in Table 2.3.

2.6.2 Model validation

In order to validate the proposed model, the results obtained from Eq. (2.6) are compared to the experimental data of Ref. [24,27]. It should be noted that test conditions A-D (given in Table 2.3) are used for generating the fouling rate constant (K) and test conditions E-G are used for model

validation. It should be noted that tests E and F are on membrane B which has a much lower vapor diffusion resistance (VDR) than membrane A which was used to determine the empirical fouling rate constant. Test F is with membrane A, but is for a longer test time (20 h). These tests will verify if the model works for different membranes and test durations. Sections 2.6.2.1 to 2.6.2.3 will address the validity of the model using the operating conditions mentioned in Table 2.3.

2.6.2.1 Test E (Membrane B, RH_{air} = 10%)

Figure 2.7 shows a comparison between predicted and the experimental normalized moisture transfer flux for a supersaturated solution at air relative humidity of 10%. Although there are some discontinuities in experimental data, there is a good agreement between predicted and experimental M* (the difference between modelling and experimental results is about ±11%). After 10 hours of operation, the model predicts a moisture transfer reduction of 60%, while the experimental data shows a reduction of 65%. In this figure, there are periodic changes in the boundary conditions (i.e., fluctuations in air relative humidity during experiments) that could have accounted for the deviations observed within the first 5 hours. Since the total uncertainty for this test condition is quite large (~40%), random uncertainty bars are depicted in Figure 2.7.

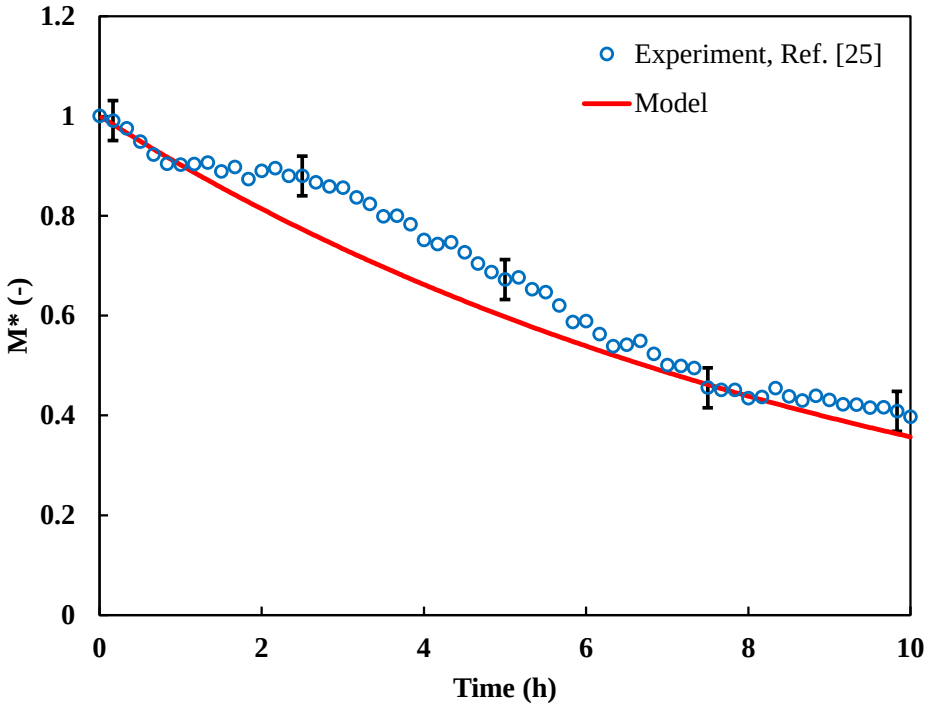

Figure 2.7. Comparison of normalized moisture transfer flux (M*) versus time between model and experiment for membrane B at RH_{air} = 10% and C* = 1.03.

2.6.2.2 Test F (Membrane B, RH_{air} = 20%)

In order to evaluate the validity of the model at another air relative humidity, a comparison between model and experiment is shown in Figure 2.8 at air relative humidity of 20% for C* = 1.03. Figure 2.8 shows that the model predicts M* versus time quite well (the difference between modelling and experimental results lies within ±6%) and the modeling results are within the uncertainty limits of the experiments. It should be noted that since the total uncertainty for this condition (~80%) is quite high due to the small change in relative humidity for the air as it flows through the LAMEE, the random uncertainty bars are shown in Figure 2.8.

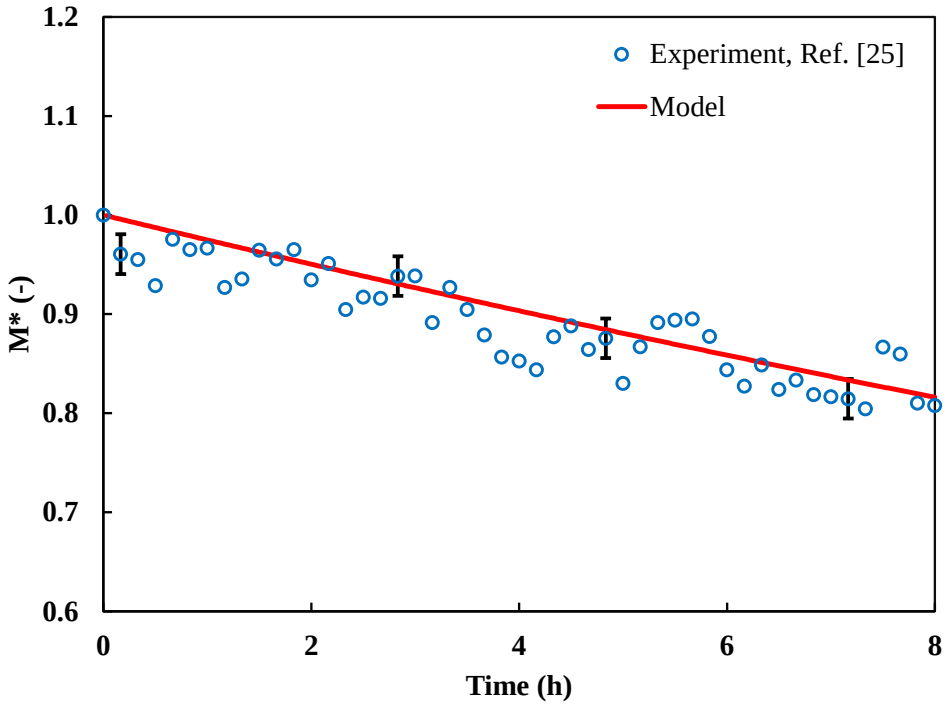

Figure 2.8. Comparison of normalized moisture transfer flux (M*) versus time between model and experiment for membrane B at RH_{air} = 20% and C* = 1.03.

It can be seen from Figure 2.8 that, based on model predictions, the decline in M* after 8 hours at air relative humidity of 20% is nearly 20% for C* = 1.03. However, the amount of decline for the same solution at air relative humidity of 10% is about 65% (Figure 2.7). The reason is that at lower air relative humidity, the difference between humidity ratio of desiccant solution and air stream increases which leads to higher moisture transfer rate. At elevated moisture transfer rates, more evaporation occurs at solution-membrane interface, which causes a rise in supersaturation at the

solution-membrane interfaces. At higher degrees of supersaturation, more crystals are prone to form and grow on the membrane surface.

2.6.2.3 Test G (Membrane A, RH_{air} = 10%, Longer test time)

In this section the model is validated with a 20-hour test to ensure that the fouling rate constant applies to longer test times. Figure 2.9 shows that the model is in a good agreement with the experimental data (a difference of about ±4% between modelling and experimental results) which confirms the ability of the model to represent the reduction in moisture transfer flux over longer periods. After 20 hours, the model predicts 76% reduction in M*, while the experimental data shows 73% reduction. Figure 2.9 shows that over the time, the growth of crystal particles covers a larger area of the membrane surface slowing down the moisture transfer through the membrane.

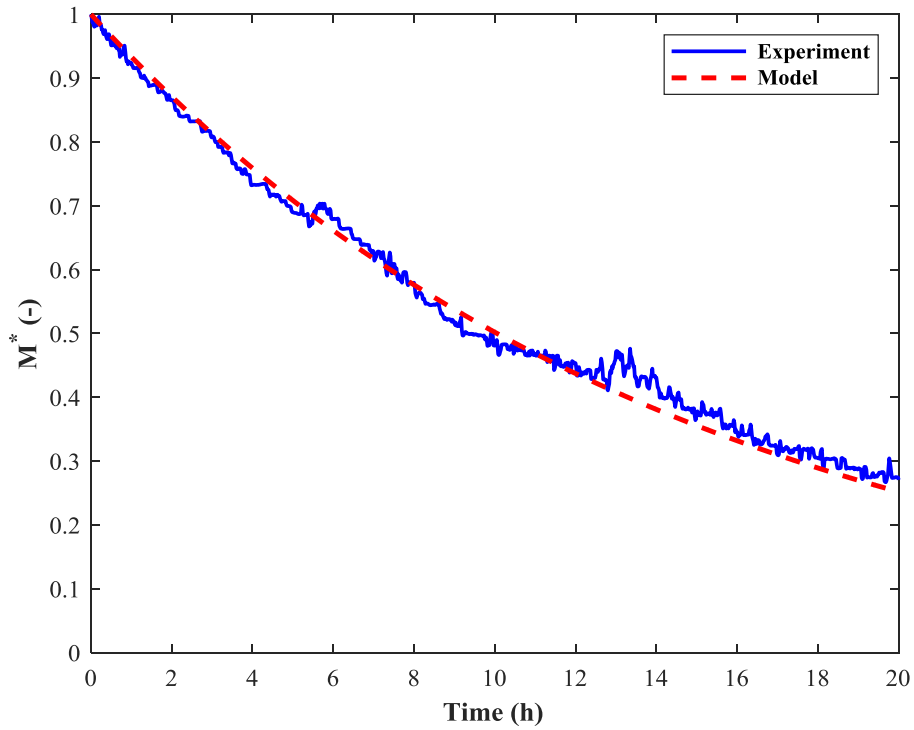

Figure 2.9. Comparison of normalized moisture transfer flux (M*) versus time between model and experiment for longer testing period at RH_{air} = 10% for C* = 1.03.

2.6.3 Sensitivity analysis

The aim of this section is to investigate the effect of the fouling rate constant (K), the convective mass transfer coefficient of the air stream ($h_{m,air}$), and vapor diffusion resistance (VDR) of the membrane on the normalized moisture transfer flux (M*). In this section, fouling will be quantified

by both the total reduction in M* at 10 hour and the rate of change of M* (i.e. the fouling rate ($\dot{m}^*$) according to Eq. (2.7)) at 0 hour.

2.6.3.1 Fouling rate constant (K)

Figure 2.10 shows the effect of the fouling rate constant (K) on the normalized moisture transfer flux (M*) and fouling rate ($\dot{m}^*$) for membrane A (VDR=97 s/m). Figure 2.10 shows that increasing K decreases M* and increases $\dot{m}^*$ as expected because increasing K increases the deposition rate (fouling rate) as per Eq. (2.3). A ±10% change in K has the greatest effect at high concentrations (±9% in M* and ±10% in $\dot{m}^*$ at C* = 1.03) and with dryer air (±22% in M* and ±10% in $\dot{m}^*$ at RH_{air} = 5%). As it can be seen, the change in K would not result in huge difference in M* and thus K determined from Eq. (2.25) can be used with confidence in the model. Figure 2.10(b) shows that the initial fouling rate ($\dot{m}^*$ at 0 hour) is about four times greater when the salt solution is supersaturated (C* = 1.03) than the fouling rate when the solution is saturated (C* = 1.0).

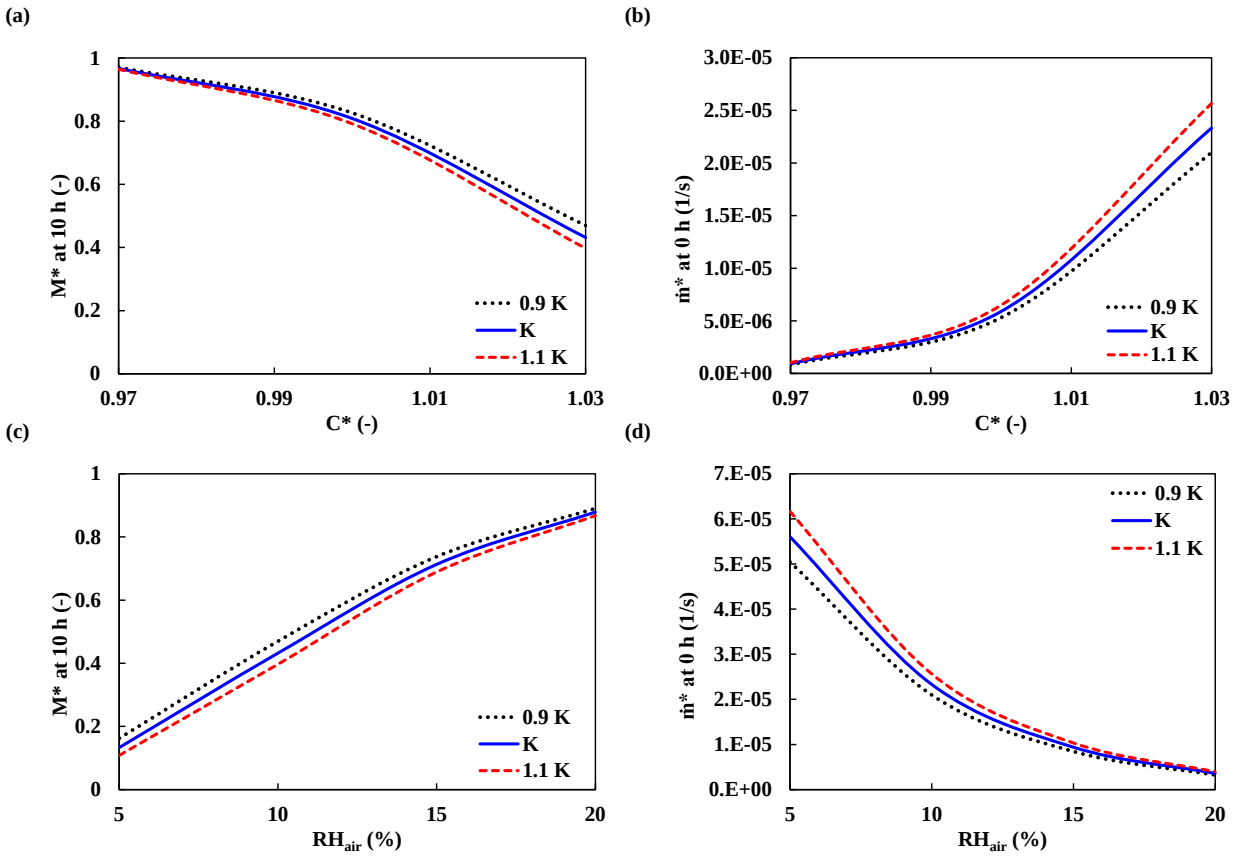

Figure 2.10. Effect of fouling rate constant on (a) normalized moisture transfer flux (M*) at 10 h versus C* at RH_{air}=10%, (b) fouling rate ($\dot{m}^*$) at 0 h versus C* at RH_{air}=10%, (c) M* at 10 h versus RH_{air} at C*=1.03, and (d) $\dot{m}^*$ at 0 h versus RH_{air} at C*=1.03.

2.6.3.2 Convective mass transfer coefficient of air

In the model, the Chilton-Colburn analogy was used to obtain the convective mass transfer coefficient of air in the LAMEE. It has been shown that this analogy may not be applicable for simultaneous heat and mass transfer in membrane energy exchangers [77]. Ghadiri Moghaddam et al. [78] developed the following correlation to determine the Sherwood number:

$$\mathrm{Sh} = \mathrm{Nu}\,\mathrm{Le}^{-(0.065\pm0.01)} \tag{2.26}$$

The above equation was used to find the convective mass transfer coefficient of air which was then applied to the model to predict M*. Moreover, a ±10% change was applied to the convective mass transfer coefficient of air to observe the variations in M*. Figure 2.11 presents the effect of the convective mass transfer coefficient of air ($h_{m,air}$) on M* and $\dot{m}^*$ for membrane A (VDR= 97 s/m). It should be noted that 0.95 $h_{m,air}$ is the convective mass transfer coefficient given by Eq. (2.26).

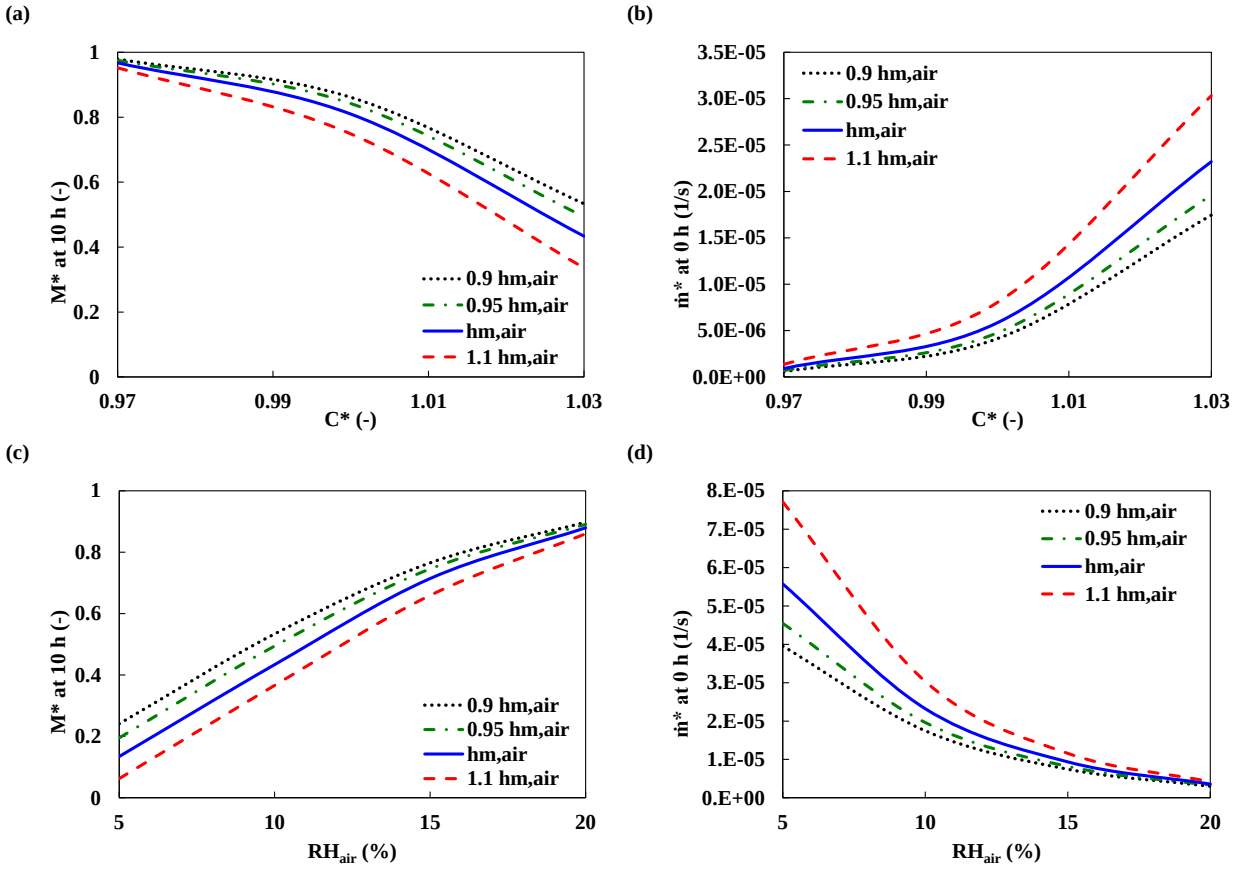

Figure 2.11. Effect of convective mass transfer coefficient of air on (a) M* at 10 h versus C* at RH_{air}=10%, (b) fouling rate ($\dot{m}^*$) at 0 h versus C* at RH_{air}=10%, (c) M* at 10 h versus RH_{air} at C*=1.03, and (d) $\dot{m}^*$ at 0 h versus RH_{air} at C*=1.03.

Figure 2.11 shows that increasing $h_{m,air}$ reduces M* and increases $\dot{m}^*$ because the rate of moisture transfer through the membrane increases as the convective mass transfer coefficient of air increases. Therefore, concentration polarization increases on the membrane surface accelerating the fouling rate. A ±10% change in $h_{m,air}$ leads to the greatest impact at higher solution concentration (±23% in M* and ±31% in $\dot{m}^*$ at C* = 1.03) and with lower air relative humidity (±54% in M* and ±40% in $\dot{m}^*$ at RH_{air} = 5%).

2.6.3.3 Vapor diffusion resistance (VDR) of the membrane

This section discusses the effect of changing membrane VDR on M* and $\dot{m}^*$ for membrane A (VDR = 97 s/m). Figure 2.12 demonstrates that the higher the membrane VDR, the lower the moisture transfer rate resulting in lower fouling rate. As it can be observed, a ±10% change in VDR has a slight effect on both M* and $\dot{m}^*$ (±4% in M* and ±6% in $\dot{m}^*$ at C* = 1.03).

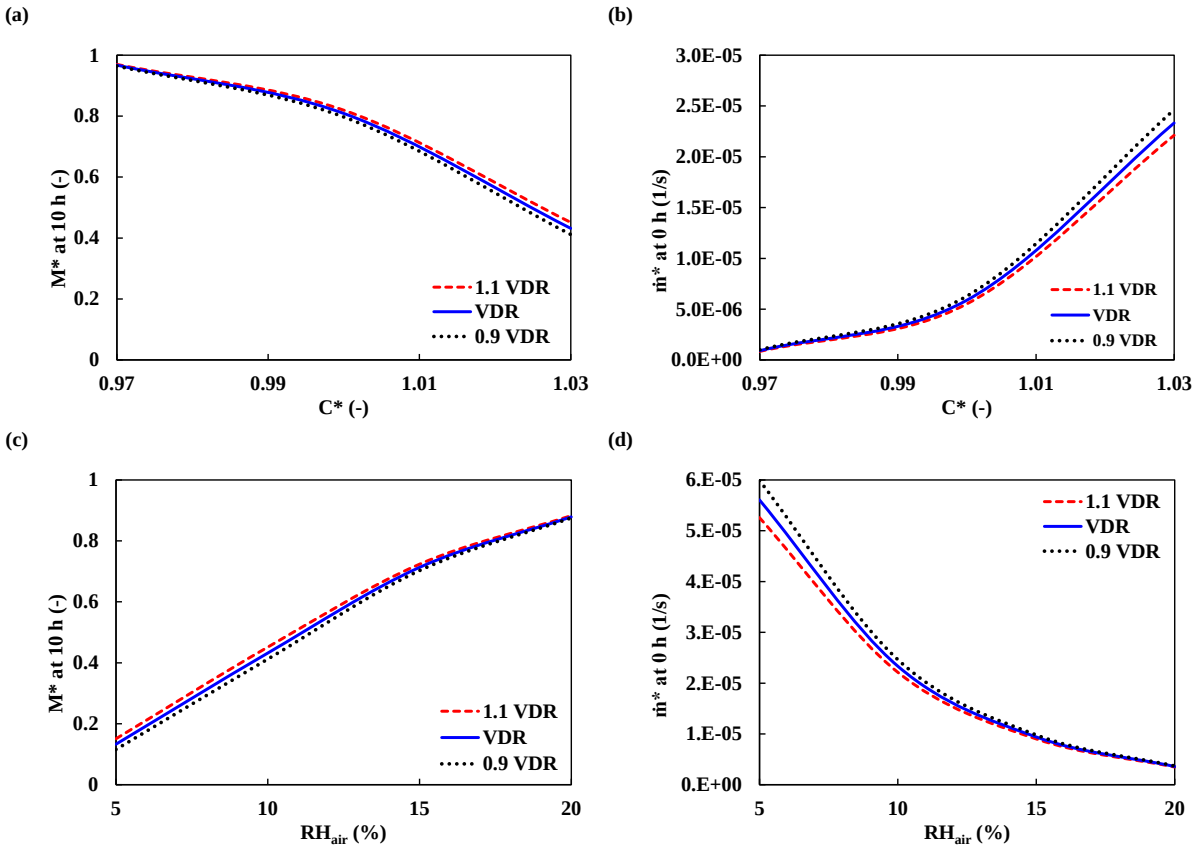

Figure 2.12. Effect of vapor diffusion resistance of the membrane on (a) M* at 10 h versus C* at RH_{air}=10%, (b) fouling rate ($\dot{m}^*$) at 0 h versus C* at RH_{air}=10%, (c) M* at 10 h versus RH_{air} at C*=1.03, and (d) $\dot{m}^*$ at 0 h versus RH_{air} at C*=1.03.

2.6.3.4 Comparison between different parameters

This section presents the comparison between the effects of various parameters on the change in normalized moisture transfer flux (M*) and fouling rate ($\dot{m}^*$). Figure 2.13 is a comparison to show the amount of change in M* and $\dot{m}^*$ by a 10% increase in the parameters specified in the x-axis for both membranes A and B. The figure represents a case where there is a higher rate of crystallization (C* = 1.03 at RH_{air} = 5% and RH_{air} = 10%). As it can be observed, the change in convective mass transfer coefficient of air has the greatest effect on both M* and $\dot{m}^*$, while the change in membrane VDR has the lowest impact. However, the magnitude of change in M* and $\dot{m}^*$ by changing the convective mass transfer coefficient of air ($h_{m,air}$) for membrane B is greater than Membrane A. It should be mentioned that as the fouling rate is proportional to the fouling rate constant (K) as per Eq. (2.7), the change in K leads to same amount of change in $\dot{m}^*$ regardless of membrane VDR.

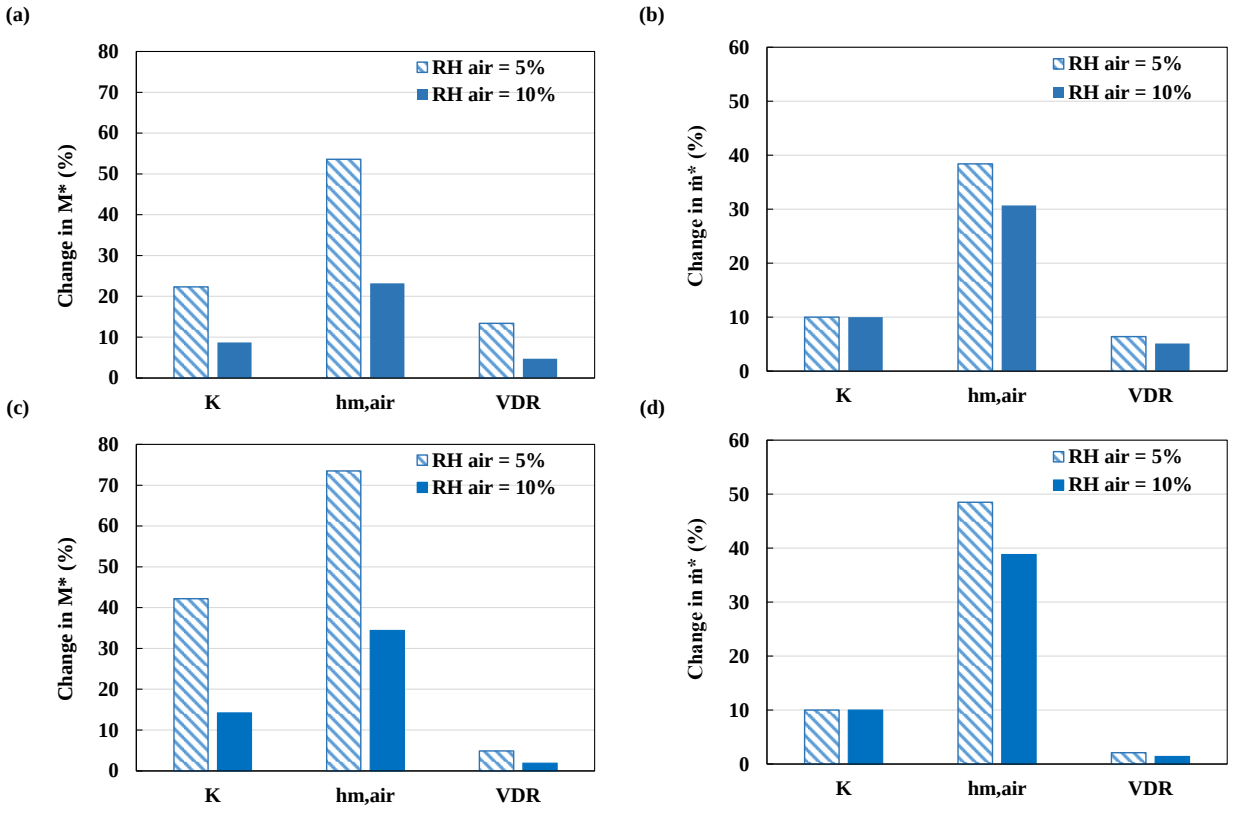

Figure 2.13. Summary of the effect of various parameters on the change in (a) M* for membrane A (VDR=97 s/m), (b) fouling rate (m *) for membrane A, (c) M* for membrane B (VDR=23 s/m), (d) m * for membrane B for a solution with C*=1.03 at RH_{air}=5% and RH_{air}=10%

2.6.4 Cleaning interval of the membrane based on model predictions

One of the beneficial points of the model is that it can predict the time when the decline in moisture transfer flux due to fouling reaches to a specific value and consequently the membrane should be replaced or cleaned. For example, if the exchanger is overdesigned by a factor of two to account for fouling, when the normalized moisture transfer flux reduces to 50% (M* = 0.5), the exchanger needs to be replaced or cleaned. Figure 2.14 presents the normalized moisture transfer flux as a function of time until M* = 0.5 at RH_{air} = 10%. As shown, M* for the desiccant solution with C* = 1.03 and membrane A declines to 0.5 after around 8 hours, while M* in case of C* = 1.0 using the same membrane reduces to 0.5 after 33 hours. The high concentration of the desiccant solution results in a deterioration in LAMEE performance due to greater amount of supersaturation and hence the adverse effects of membrane surface blockage. Similar findings have been reported in the literature for the membrane distillation systems [54,79].

Figure 2.14 also shows that for a constant solution concentration (e.g. C* = 1.03), the moisture transfer through membrane B declines to 50% earlier than through membrane A. The major reason is that membranes with low VDR cause higher rates of moisture transfer and thus lead to more severe growth of crystal particles on the membrane surface. As a result, the cleaning intervals for membranes with lower VDR is greater than the intervals for membranes with higher VDR. It can be seen from Figure 2.14 that the time to reach to M*=0.5 for a saturated solution is around fourfold the time for a supersaturated solution.

Figure 2.15 shows the time needed to reach M* equal to 50% for a saturated and supersaturated solution when VDR changes from 1 to 500 s/m and air relative humidity is 10%. The figure shows that the time to reach to half of the initial moisture transfer flux for supersaturated solutions would be shorter than the time for a saturated solution. Furthermore, increasing VDR leads to a remarkable effect on the time for a saturated solution. The time increases by a factor of 4 at C* = 1.03 and a factor of 6 at C* = 1 when VDR changes from 100 to 500 s/m. This is because at lower solution concentrations, the tendency for nucleation and crystal growth on the membrane surface decreases. As the membrane VDR increases, this tendency would be much lower due to lower rates of moisture transfer. It should be mentioned that increasing the membrane VDR is a beneficial point once fouling is under consideration. On the other hand, one limitation is a reduction in effectiveness due to reduced rate of moisture transfer through the membrane.

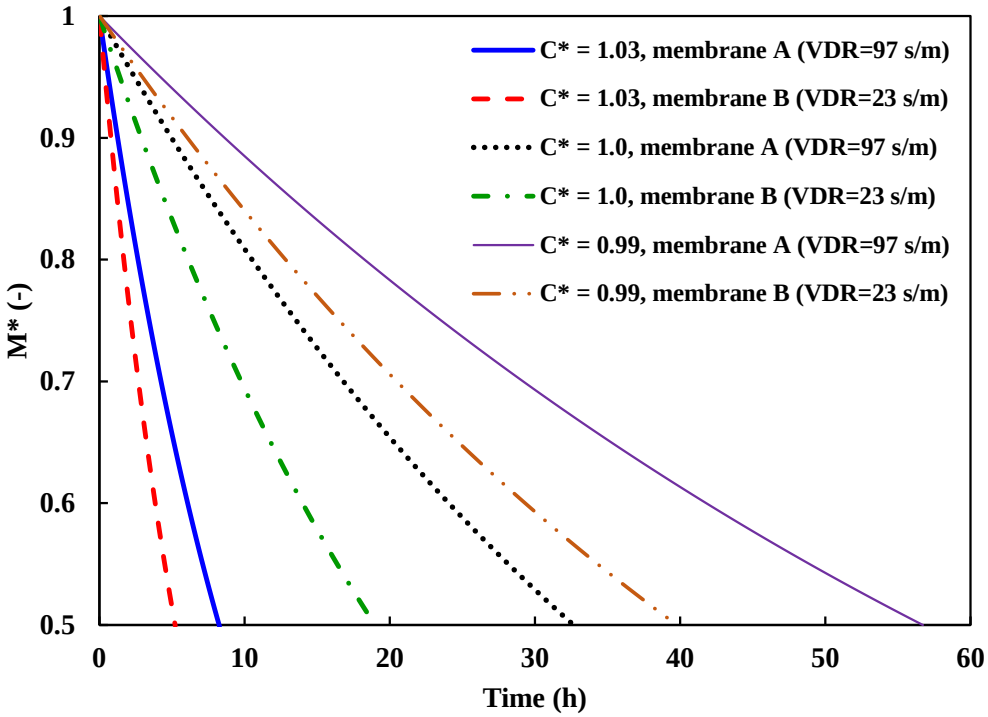

Figure 2.14. Variations of normalized moisture transfer flux (M*) versus time for three solution concentrations and two different membranes at RH_{air} = 10%.

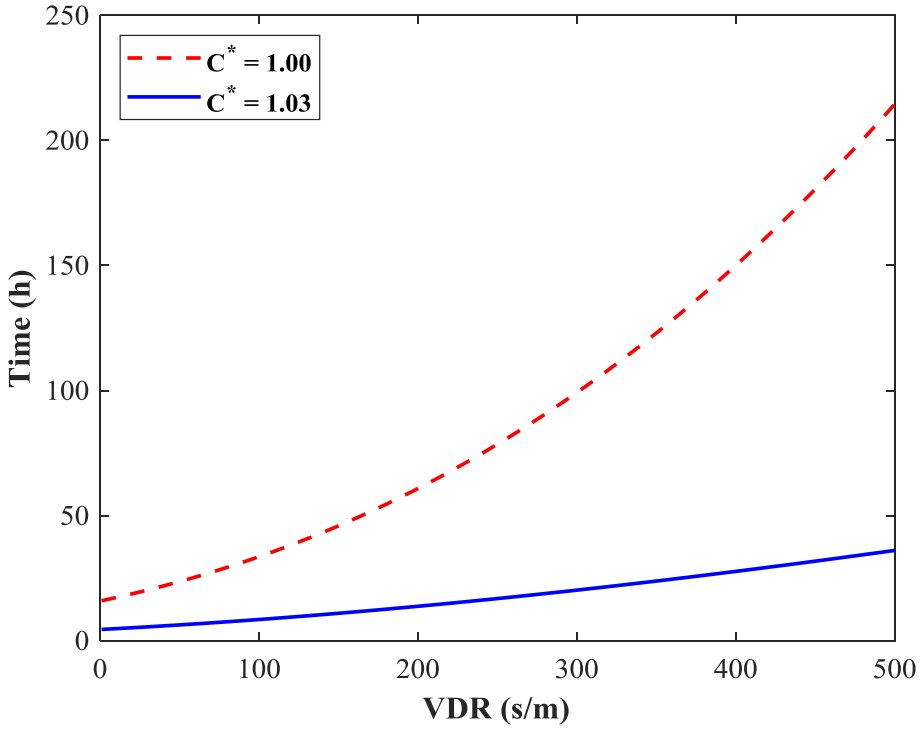

Figure 2.15. Time to reach M* = 0.5 versus VDR for a solution with C* = 1.0 and C* = 1.03 at RH_{air} = 10%.

2.6.5 Theoretical crystallization fouling

Regarding the proposed procedure in section 2.4.3 to find the desiccant solution concentration on the membrane surface, it would be possible to theoretically predict the crystallization fouling limits. Once the solution concentration at the solution-membrane interface attains the saturation concentration, the crystal particles can be formed on the surface. Figure 2.16 presents the limits of crystallization fouling for different design and operating conditions for the $MgCl_2$ solution. In the figure, any point above the line for a specific membrane, will result in saturation at the membrane surface and crystallization fouling is likely. For the points below a given line, saturation will not occur and fouling is unlikely. Care should be given to the operating conditions where the point is far above a line for a specific membrane as the LAMEE is prone to severe crystallization fouling.

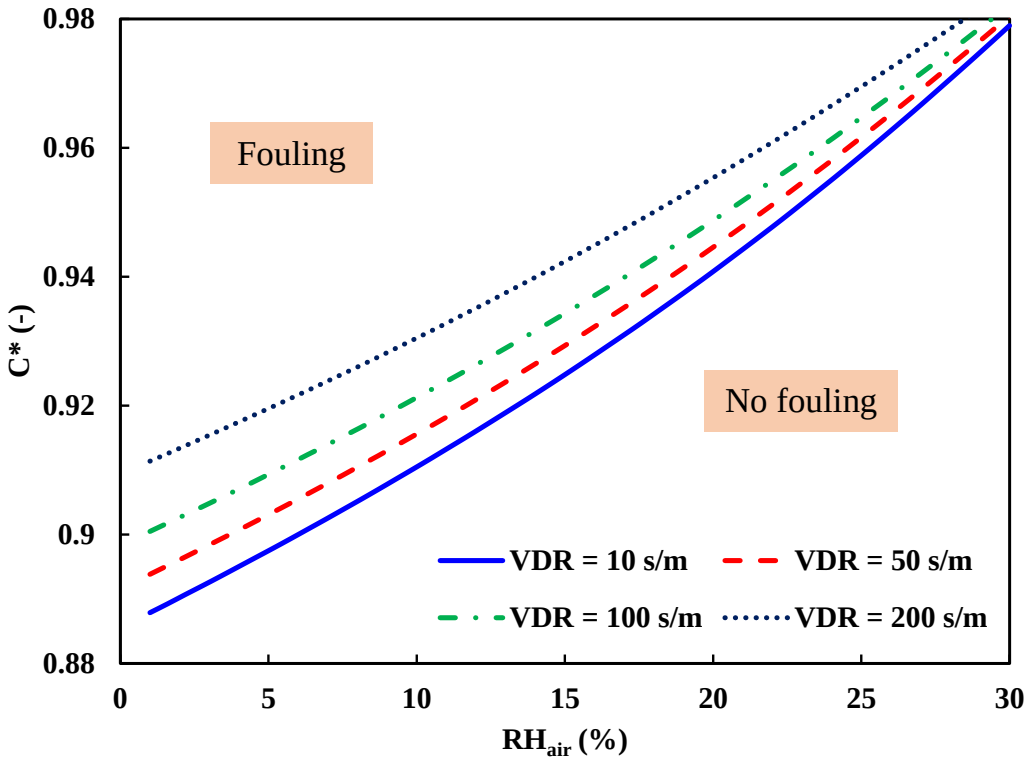

Figure 2.16. Crystallization fouling limits as a function of air relative humidity (RH_{air}) and dimensionless solution concentration (C*) for different values of vapor diffusion resistance (VDR).

2.6.6 Predicting fouling for long-term operation

This section presents the effect of fouling on the normalized moisture transfer flux (M*) after long-term operations. Figure 2.17 shows the time when normalized moisture transfer flux declines to

0.5 for a range of C* values and four different membrane VDRs. The figure shows that as C* approaches the fouling limit (e.g. C* = 0.91 for VDR = 10 s/m and C* = 0.94 for VDR = 200 s/m at RH_{air} = 10%) the cleaning interval becomes very long and the LAMEE may not need cleaning even after several years of operation.

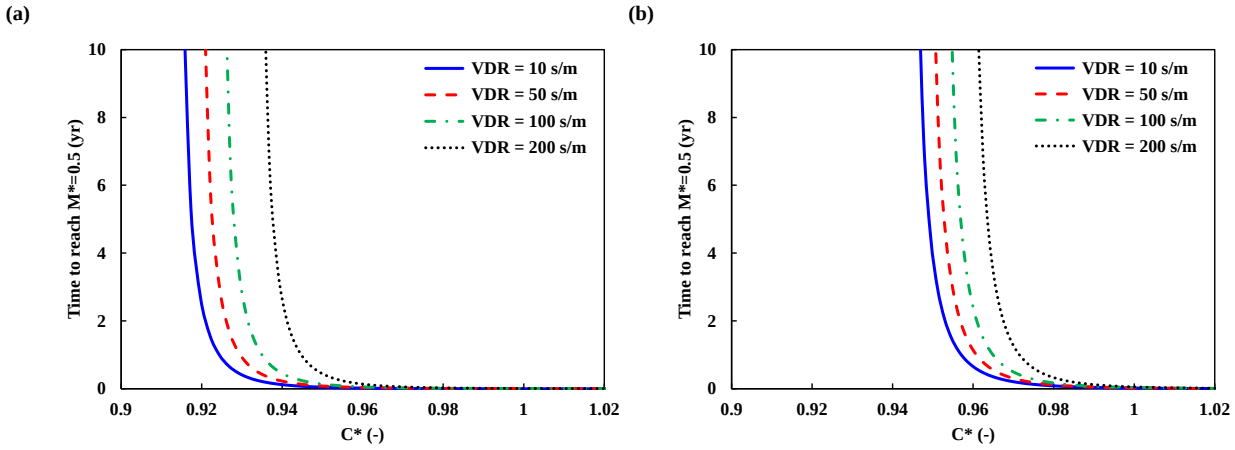

Figure 2.17. Time to reach M* = 0.5 versus C* at (a) RH_{air} = 10% and (b) RH_{air} = 20% for different vapor diffusion resistance (VDR) values.

Figure 2.18 shows the maximum C* that is allowed so that the LAMEE can operate for a certain length of time before cleaning is needed. It should be noted that in this figure the cleaning interval is defined as when the normalized moisture transfer flux (M*) is reduced by 50%. As it can be seen, the maximum C* increases by an increase in membrane VDR. Moreover, if longer cleaning intervals are needed, low solution concentrations should be used.

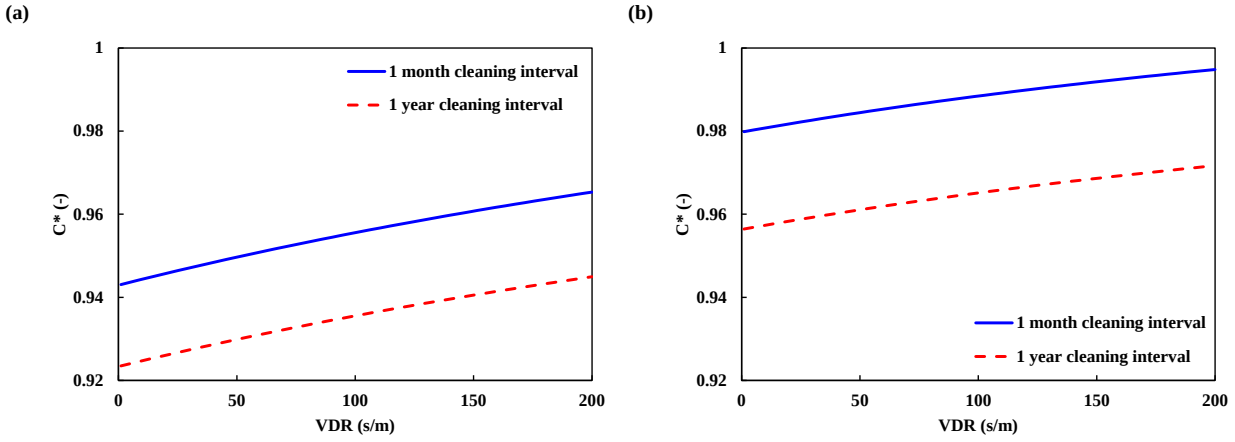

Figure 2.18. Maximum C* versus membrane VDR for two cleaning intervals at (a) RH_{air} = 10% and (b) RH_{air} = 20%.

2.7 Conclusions

In this chapter, a semi-empirical model was developed to predict the effect of crystallization fouling on the moisture transfer rate through a liquid-to-air membrane energy exchanger (LAMEE) to meet the first objective of this thesis. The model consisted of a physical model to determine the solution concentration at solution-membrane interface and an empirical model which is based on an empirical fouling rate constant that was determined using non-linear regression of experimental data. Some data are used to create the empirical constant and others are used to validate the model. Some significant findings of this chapter include:

1- The difference between modelling and experimental results ranges from ±4% to ±11% indicating good agreement between model and experiment.
2- The experimental and numerical results show that the formation and growth of crystal particles on the membrane surface reduce the moisture transfer rate through the membrane. The model predicts that the decline in moisture transfer rate after 10 hours is about 20% at an air relative humidity of 10% and about 65% at an air relative humidity of 20% when the solution is 3% above saturation.
3- The sensitivity analysis showed that changing the fouling rate constant of a membrane by ±10% will have only a slight influence on the moisture transfer rate (±9%) and fouling rate (±10%) for a solution concentration of 3% above saturation. It was shown that increasing the convective mass transfer coefficient of air by 10% could have quite a great impact on the reduction in the moisture transfer rate (~23%) and the increase in fouling rate (~31%).
4- Based on model predictions, the initial fouling rate of a supersaturated solution (3% above saturation) is nearly four times greater than the fouling rate in case of a saturated solution.
5- The model predicts that the time required for the moisture transfer rate for a saturated solution to decline to half of its initial value, which is defined as the cleaning or replacement interval for the membrane, is four times greater than for a supersaturated solution (3% above saturation).
6- As the solution concentration reaches to its fouling limit, the cleaning or replacing of the membrane may not be required for several years.

The next chapter will focus on modifying the current model to determine the operating conditions where there is a risk of crystallization fouling.

CHAPTER 3

CRYSTALLIZATION FOULING LIMITS IN COUNTER-FLOW LAMEES

3.1 Overview

In this chapter, the fouling model developed in Chapter 2 is expanded to model a practical LAMEE with a flowing solution stream rather than a LAMEE with stagnant solution. The model is then used to determine the critical points where fouling is most likely to occur in a LAMEE under various operating conditions. The concept is that once supersaturation is reached at any point in a LAMEE for a given operating and design condition, there will be a risk of crystal formation and growth.

This chapter contains a manuscript submitted to the ASME Journal of Heat Transfer. The four authors who made a contribution to this chapter are Alireza Razmavar (M.Sc. student) who developed the model and prepared the original manuscript, Dr. Gurubalan Annadurai (Postdoctoral Fellow), Dr. Adesola Olufade (Co-supervisor), and Professor Carey Simonson (Supervisor) who critically reviewed the manuscript.

A theoretical study on crystallization fouling limits in liquid-to-air membrane energy exchangers

Alireza Razmavar, A. Gurubalan, Adesola Olufade, Carey J. Simonson

3.2 Abstract

Crystallization fouling is a major hurdle for the efficient performance of membrane-based separation systems operating with aqueous salt solutions. Liquid-to-air membrane energy exchangers (LAMEEs) are a newly emerging equipment that use micro-porous membranes to separate aqueous salt solutions and air streams while enabling simultaneous heat and moisture transfer between the streams. LAMEEs may be prone to crystallization fouling in some specific operating and/or design conditions. A theoretical crystallization fouling limit model is developed in this chapter to predict at which conditions crystallization is likely to happen for a given LAMEE. The results of fouling limit model provides insight into how the design parameters and operating conditions affect crystallization fouling of LAMEEs. Then, using the semi-empirical model developed in the previous chapter, the behavior of moisture transfer flux through the membrane is discussed for a LAMEE operating with magnesium chloride at different operating conditions. The results show that increasing the desiccant temperature, decreasing the heat capacity ratio and decreasing the vapor diffusion resistance of the membrane increases the risk of crystallization fouling.

3.3 Introduction

Membrane-based separation technologies such as membrane distillation, reverse osmosis and forward osmosis rely on using porous membranes and a driving force to separate water from an aqueous solution [80-82]. LAMEEs are exchangers which simultaneously transfer heat and moisture between an air stream and a desiccant solution stream through a semi-permeable membrane [30]. The driving potential in LAMEEs for moisture transfer is vapor pressure gradient between the streams. The indirect contact between air and desiccant solution in LAMEEs would make them beneficial in wide-ranging applications such as residential buildings, commercial buildings, hospitals, and data centers. Aqueous solutions of halide salts such as $MgCl_2$ and LiCl are used as desiccant solutions in LAMEEs [41].

One major obstacle in the application of LAMEEs is crystallization fouling of the membrane. In some specific operating conditions, when water transfers from the liquid side to the air side, the aqueous salt solution may become saturated. Therefore, there is a risk of crystal formation/growth on the membrane surface or within the membrane pores. The crystals formed on the membrane surface generate additional resistance for the mass transfer as shown in Chapter 2, thus leading to a reduction in moisture transfer rate through the membrane which increases energy consumption, membrane cleaning cycles, and material costs [4].

Given that there is paucity of research on crystallization fouling of LAMEEs in the open literature, recent review papers [47,83] have stated that rigorous research studies are needed to better understand fouling in LAMEEs. Several experimental studies have been performed on fouling of membrane energy exchangers which include fouling detection methods, fouling characterization and fouling reversal [22–27]. However, there is no theoretical study specifically focused on fouling of membrane energy exchangers. Only in one part of a study on fouling of a membrane evaporative cooling system, a theoretical parameter was developed as a criterion to interpret the extent of fouling under different experimental conditions [21].

It is essential to know the fouling limit of a LAMEE so that crystallization fouling can be avoided. To the best knowledge of the authors, only two studies have discussed crystallization fouling limits; one study in membrane distillation [53] and the second study in run-around membrane energy exchangers [84]. In the first study, a theoretical model was developed to predict the regions where fouling is unlikely to happen in terms of design and operating conditions [53]. In the second study, the risk of crystallization fouling was investigated for various desiccant solutions and climate conditions [84]. The findings showed that $MgCl_2$(aq) is the most susceptible desiccant solution to crystallization fouling. As mentioned before, there is a high likelihood of crystallization fouling in some specific cases. For example, in the liquid desiccant loop, the diluted solution from dehumidifier is dried in the regenerator section where the solution concentration increases and crystallization may occur at some point across the LAMEE.

To date, there is not any study available in the literature to determine the crystallization fouling limits in LAMEEs. Therefore, the main goal of this chapter is to develop a model that can be used to determine fouling limits in LAMEEs, which can be used to provide insight into preventing crystallization fouling.

This chapter will first present the development of a crystallization fouling limit model for a counter-flow LAMEE. The fouling limits will be presented for three different desiccant solutions, i.e. $MgCl_2$(aq), $CaCl_2$(aq), and LiCl(aq), at various design parameters and operating conditions. Afterwards, the reduction in moisture transfer flux through the membrane due to fouling will be addressed for a LAMEE that utilizes $MgCl_2$(aq) as its working fluid.

3.4 Description of fouling limit model

3.4.1 Physical model

A schematic of a counter-flow LAMEE is shown in Figure 3.1. The dry air passes below the hydrophobic membrane and the desiccant solution flows on top of the membrane. In the case of drying the desiccant solution, the concentration of the solution will be highest at the outlet of desiccant solution. Therefore, crystallization fouling is expected to initiate at the outlet of desiccant solution and possibly moves towards the inlet with time. In this chapter, the fouling limit is defined when the concentration at the solution-membrane interface reaches saturation at the outlet of the LAMEE. To develop the fouling limit model, saturation conditions are used at solution-membrane interface at the LAMEE outlet when the inlet conditions of desiccant solution are varied.

The dimensions of the LAMEE used in Ref. [85] are applied to this study and are presented in Table 3.1. It should be noted that since the length and width of the membrane are greater than the thickness, the heat and mass transfer are assumed to be one-dimensional.

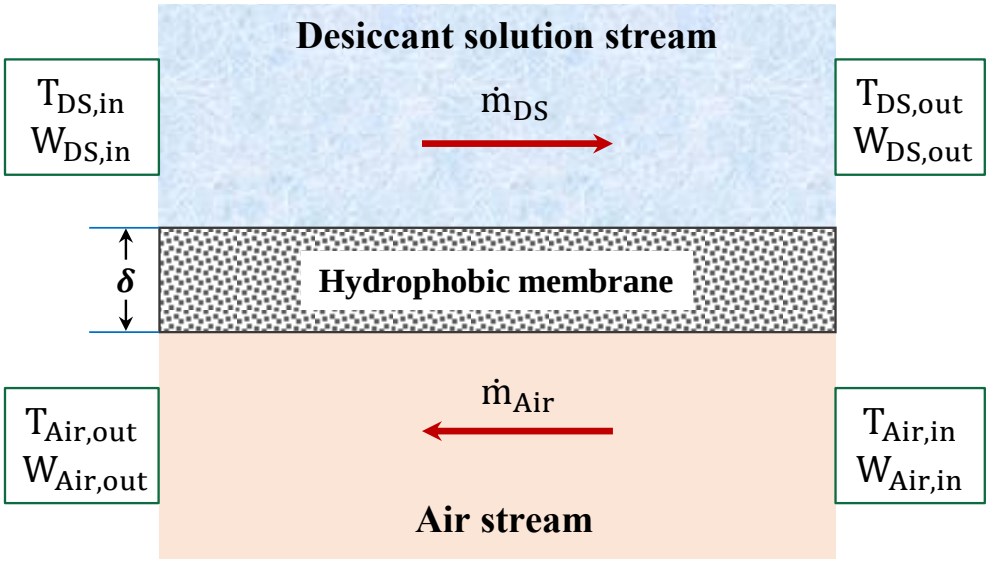

Figure 3.1. A schematic diagram of the counter-flow LAMEE.

Table 3.1. Specifications of the counter-flow LAMEE that is used in this chapter [85].

Parameter	**Value**
Exchanger length (m)	0.99
Exchanger aspect ratio of the air-liquid contact area (-)	10.5
Air gap thickness (mm)	5
Solution gap thickness (mm)	1.2
Vapor diffusion resistance of membrane (s/m)	24
Membrane thermal conductivity (W/mK)	0.065
Membrane thickness (mm)	0.265

3.4.2 Theoretical model

The aim of the model is to determine the concentration of desiccant solution at the inlet of the LAMEE that result in saturation of the desiccant solution at the solution-membrane interface at the outlet of the LAMEE. The energy and mass conservation equations are used to find the fouling limits.

The energy conservation equations for the desiccant and air streams are given in Eq. (3.1) and (3.2), respectively. These equations are as follows:

$$UA\Delta T_{lm} = \dot{m}_{DS} c_{p,DS} (T_{DS,in} - T_{DS,out}) \tag{3.1}$$

$$UA\Delta T_{lm} = \dot{m}_{air} c_{p,air} (T_{air,out} - T_{air,in}) \tag{3.2}$$

where U is the convective heat transfer coefficient which will be defined later on, A is the total area of the membrane, c_p is the specific heat capacity, $\dot{m}$ is the mass flow rate and ΔT_{lm} is the log mean temperature difference defined as:

$$\Delta T_{lm} = \frac{\Delta T_2 - \Delta T_1}{\ln\left(\frac{\Delta T_2}{\Delta T_1}\right)}, \tag{3.3}$$

$$\Delta T_1 = T_{DS,in} - T_{air,out} \tag{3.4}$$

$$\Delta T_2 = T_{DS,out} - T_{air,in} \tag{3.5}$$

The inlet temperature of air ($T_{air,in}$) and desiccant solution ($T_{DS,in}$) are known. Solving Eq. (3.1) to (3.5) can give the outlet temperature of the air ($T_{air,out}$) and desiccant solution ($T_{DS,out}$).

The overall heat transfer coefficient in Eq. (3.1) and (3.2) is calculated by:

$$U = \left(\frac{1}{h_{air}} + \frac{\delta}{k_{mem}} + \frac{1}{h_{DS}}\right)^{-1} \tag{3.6}$$

h in the above equation represents the convective heat transfer coefficient which is obtained from the definition of Nusselt number as follows:

$$h = \frac{Nuk}{D_h} \tag{3.7}$$

The Nusselt number of 5.39 is used for both the air and desiccant solution for a fully developed laminar flow between two infinite parallel plates with one wall insulated and the other wall with constant heat flux [34].

In order to find the solution concentration at the inlet which may trigger crystallization fouling at the outlet, it is assumed that the solution concentration on the membrane surface at the outlet is saturated. The solution concentration at the outlet can then be calculated using the mass balance equation at solution-membrane interface and the equation is given by [69]:

$$U_m(W_{DS,mem,out} - W_{air,in}) = h_{m,DS}(C_{DS,mem,out} - C_{DS,out}) \tag{3.8}$$

where U_m, h_m, and C are the overall mass transfer coefficient, the convective mass transfer coefficient, and the solution concentration, respectively. The subscripts DS, DS, mem, and air represent desiccant solution, desiccant solution on the membrane, and air, respectively. $W_{DS,mem}$ in Eq. (3.8) is the humidity ratio in equilibrium with the desiccant solution at the interface between membrane and solution which is a function of the desiccant solution concentration and solution temperature at the membrane surface. W_{DS} at any location can be expressed as [70]:

$$W_{DS} = 0.62198\frac{p_v}{P - p_v} \tag{3.9}$$

where P is the total pressure and p_v is the partial pressure of water vapor given by [71]:

$$p_v = a_w p_{v,sat} \tag{3.10}$$

where a_w is the solution water activity, which is a function of solution concentration, that can be calculated from the correlations given in Table 3.2. $p_{v,sat}$ in Eq. (3.10) is the saturation pressure of pure water that can be found using the Antoine equation where $p_{v,sat}$ is calculated in Pa based on temperature T in Kelvin [71]:

$$p_{v,sat} = \exp\left(23.5377 - \frac{4016.3632}{T - 38.6339}\right) \tag{3.11}$$

$W_{DS,mem,out}$ is calculated using Eq. (3.9) and applying it to Eq. (3.8) gives solution concentration at the outlet ($C_{DS,out}$) when the concentration at the solution-membrane interface at the outlet ($C_{DS,mem,out}$) is saturated. Once $C_{DS,out}$ is calculated, using Eq. (3.9) to (3.11) gives the equivalent humidity ratio of air in equilibrium with the desiccant solution at the outlet ($W_{DS,out}$).

Table 3.2. Correlations for water activity of different desiccant solutions.

Desiccant solution	**Water activity (a_w)**	**Ref.**
$MgCl_2$(aq)	$a_w = 0.00018b^4 + 0.00021b^3 - 0.0206b^2 - 0.0375b + 0.9996$	[72]
$CaCl_2$(aq)	$a_w = -0.0000275b^5 + 0.00051b^4 - 0.0012b^3 - 0.016b^2 + 0.026b + 0.9994$	[72]
LiCl(aq)	$a_w = 0.0016b^2 - 0.07b + 0.9996$	[86]

Note: b is the solution molality given as: $\frac{1000\times((C_{DS}/10)/MW)}{100-(C_{DS}/10)}$ where MW is the molecular weight of the solution.

Eq. (3.12) and (3.13) are then used to find the remaining parameters, which are the humidity ratio of air at the outlet ($W_{air,out}$) and humidity ratio of the solution at the inlet ($W_{DS,in}$).

$$U_m A \Delta W_{lm} = \dot{m}_{DS}(W_{DS,in} - W_{DS,out}) \tag{3.12}$$

$$U_m A \Delta W_{lm} = \dot{m}_{air}(W_{air,out} - W_{air,in}) \tag{3.13}$$

where ΔW_{lm} is the log mean humidity ratio difference.

By solving Eq. (3.12) and (3.13), $W_{DS,in}$ can be calculated and then using Eq. (3.9) yields $C_{DS,in}$. The inlet solution concentration can be dimensionalized using the following equation:

$$C^*_{DS,in} = \frac{C_{DS,in}}{C_s} \tag{3.14}$$

where C_s is the saturation concentration of solution. A flowchart for calculating the concentration of desiccant solution at the inlet ($C_{DS,in}$) is shown in Figure 3.2.

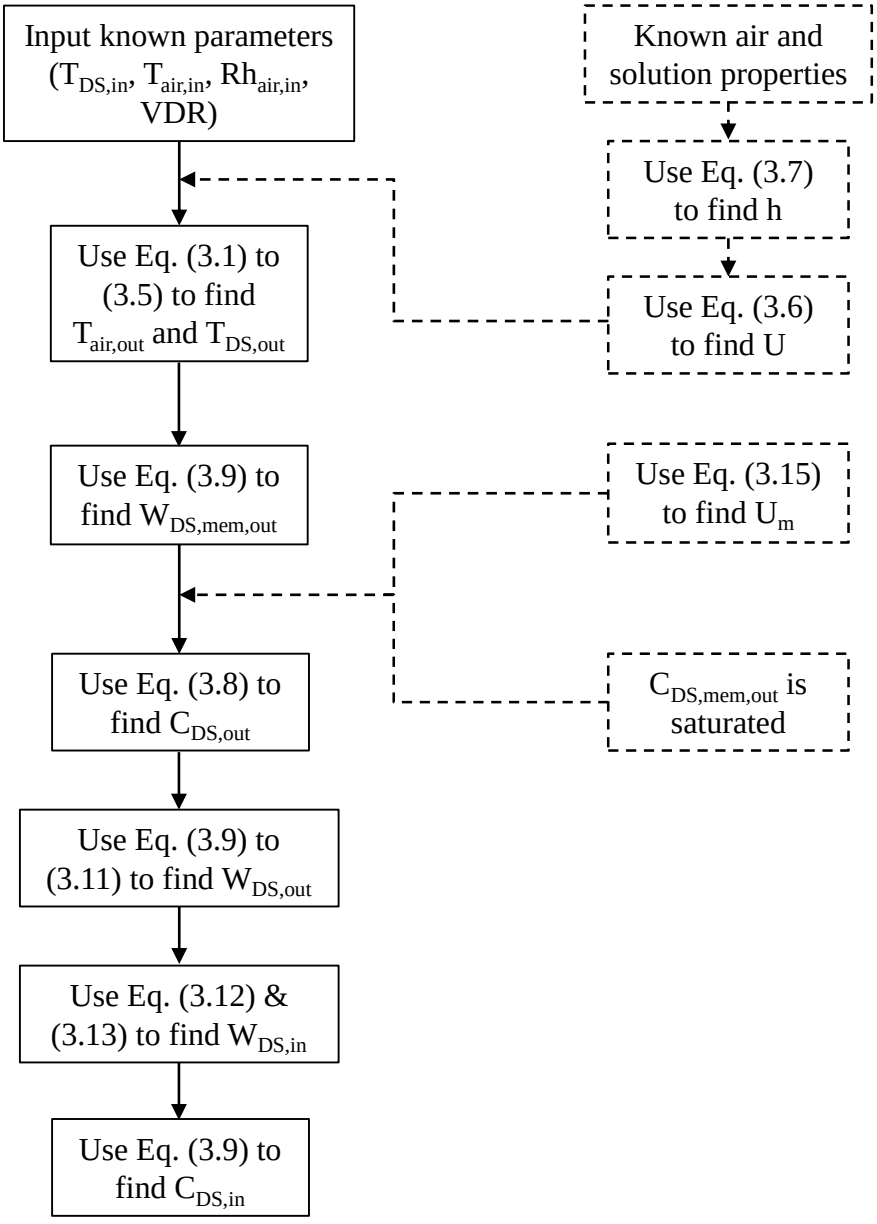

Figure 3.2. Flowchart for calculating the concentration of desiccant solution at the inlet ($C_{DS,in}$).

The overall mass transfer coefficient in Eq. (3.8), (3.12), and (3.13) is determined by [69]:

$$U_m = \left(\frac{1}{h_{m,air}} + \frac{R_{mem}}{\rho_{Air}}\right)^{-1} \tag{3.15}$$

The convective mass transfer coefficient of air ($h_{m,air}$) in Eq. (3.15) and convective mass transfer coefficient of solution ($h_{m,DS}$) in Eq. (3.8) are determined using the Chilton-Colburn analogy defined as [74]:

$$\frac{h}{h_m} = c_p Le^{2/3} \tag{3.16}$$

where c_p is the specific heat capacity of air or solution and Le is the Lewis number. It should be noted that Le for air is about 1 but for the desiccant solution is calculated using the following equation:

$$Le = \frac{k}{\rho c_p D_{AB}} \tag{3.17}$$

where k is the thermal conductivity, ρ is density, and D_{AB} is diffusion coefficient. It is worth mentioning that all these thermophysical properties (k, ρ, and D_{AB}) for various desiccant solutions used in this study are given in Ref. [87] and are listed in Table 3.3.

In this chapter, the non-dimensional parameters, i.e. NTU, NTU_m, and Cr* are used in the model to present the results. These parameters are defined as follows:

$$NTU = \frac{UA}{(\dot{m}c_p)_{min}} \tag{3.18}$$

$$NTU_m = \frac{U_m A}{(\dot{m})_{min}} \tag{3.19}$$

and

$$Cr^* = \frac{(\dot{m}c_p)_{sol}}{(\dot{m}c_p)_{air}} \tag{3.20}$$

where Cr* represents the heat capacity ratio, sol and air represent the solution and air, respectively.

Table 3.3. Thermophysical properties of studied desiccant solutions.

Desiccant solution	Thermophysical properties
$MgCl_2$(aq)	$\log \rho = \log \rho_0 + (0.35238 - 34.5E-6T^2)0.001C_{DS}$ $C_p = C_{p,w} + (-6304.3 + 3.083C_{DS} + 7.9T - 0.0139T^2)0.001C_{DS}$ $k = k_0(1 - 478E - 6C_{DS})$ $D_{AB} = 10^{-11} \times (103 + 3.84b + 6.4b^2 - 3.86b^3 + 0.4b^4)$
$CaCl_2$(aq)	$\log \rho = \log \rho_0 + (0.3627 + 14E - 8T^2)0.001C_{DS}$ $C_p = C_{p,w} + (-6360.2 + 4.706C_{DS} + 7.2T - 0.0125T^2)0.001C_{DS}$ $k = k_0(1 - 182E - 6C_{DS})$ $D_{AB} = 10^{-11} \times (111 + 4.31b + 9.69b^2 - 4.09b^3 + 0.335b^4)$
LiCl(aq)	$\log \rho = \log \rho_0 + (0.2452 + 1.9E - 8T^2)0.001C_{DS}$ $C_p = C_{p,w} + (-5016.3 + 4.249C_{DS} - 3.4T - 0.0159T^2)0.001C_{DS}$ $k = k_0(1 - 344.5E - 6C_{DS})$ $D_{AB} = D_w \left[1 - \left(1 + \left(\frac{\sqrt{0.001C_{DS}}}{0.52}\right)^{-4.92}\right)^{-0.56}\right]$

Note: ρ_0 is the density of pure water, k_0 is the thermal conductivity of pure water given as: $k_0 = 0.5545 + 0.00246T - 0.00001184T^2$ and $C_{p,w}$ is the heat capacity of pure water given as: $C_{p,w} = 134225(T/100)^{-6.5} + 3490(T/100)^{0.14}$ where T is temperature in °C.

3.4.2.1 Decline in moisture transfer flux due to fouling for $MgCl_2$(aq)

The semi-empirical model developed in chapter 2 will be used to estimate the decline in moisture transfer flux due to fouling for $MgCl_2$(aq) for non-isothermal conditions. The model can predict the decline in moisture transfer flux at every point along the LAMEE based on the concentration and temperature at that point. For every known inlet condition, Eq. (3.1) to (3.13) are coupled to

find the solution concentration and temperature on the membrane surface at each point along the LAMEE. As mentioned in Eq. (2.6) in Chapter 2, the normalized moisture transfer flux (M*) is calculated by:

$$M^* = 1 - (1 - \exp[-K\left(C_{DS,mem} - C_s\right)^2 t] \tag{3.21}$$

where K is the fouling rate constant obtained by:

$$K = 5 \times 10^{-10} {S_{mem}}^{41.7} \tag{3.22}$$

where S_{mem} is the supersaturation degree on the membrane surface defined as:

$$S_{mem} = \frac{C_{DS,mem}}{C_s} \tag{3.23}$$

3.5 Model validation

In this section the model is validated using available experimental data in the literature. Ge et al. [32] investigated the effect of different parameters on the regeneration process of LAMEEs using LiCl(aq) and suspected that the discrepancy between their experimental and analytical data was due to crystallization fouling.

Figure 3.3 shows a comparison between the theoretical fouling limit and some test conditions of Ref. [32], as specified in Table 3.4. In this figure, crystallization fouling is likely to occur for the points above the line, like point D. However, crystallization fouling is unlikely for points that are below the line (like points A–C). It should be noted that in the study of Ref. [32], it was not specifically reported which point is exposed to crystallization fouling. It was only stated that the discrepancy between the experimental and analytical data might be due to the crystal formation because their model assumed no fouling and therefore the discrepancy will grow as fouling increases. Ge et al [32] also mentioned that at higher inlet concentrations of desiccant solution (like point D in Figure 3.2) there is a higher risk of crystallization fouling. Based on the modeling results of this chapter, the agreement between model and experimental data of Ref. [32] is the best for point D which is above the fouling limit line implying that model validity is better at high solution concentrations. Even though points A–C are below the fouling limit line, there might be some sites for crystal formation and growth during the regeneration process and thereby creates a

discrepancy in the data. It is worth mentioning that the study of Ref. [32] also suggested that membrane deflection at higher solution temperature may add to this discrepancy.

Table 3.4. Experimental test conditions used for model validation.

Test	$\dot{m}_{air}$ (kg/h)	$W_{air,in}$ (g/kg)	$RH_{air,in}$ (%)	$T_{air,in}$ (°C)	$T_{DS,in}$ (°C)	$C^*_{DS,in}$	Cr*	NTU	R_w (10^{-3})
A	5.34	14.2	51%	30	45	0.669	4	5	2.26
B	5.34	13.9	49%	29.9	50.1	0.661	4	5	3.59
C	5.33	14.6	53%	30	55.1	0.656	4	5	4.96
D	5.34	14.4	52%	30.1	55.1	0.754	4	5	2.81

Note: R_w is the moisture flux ratio.

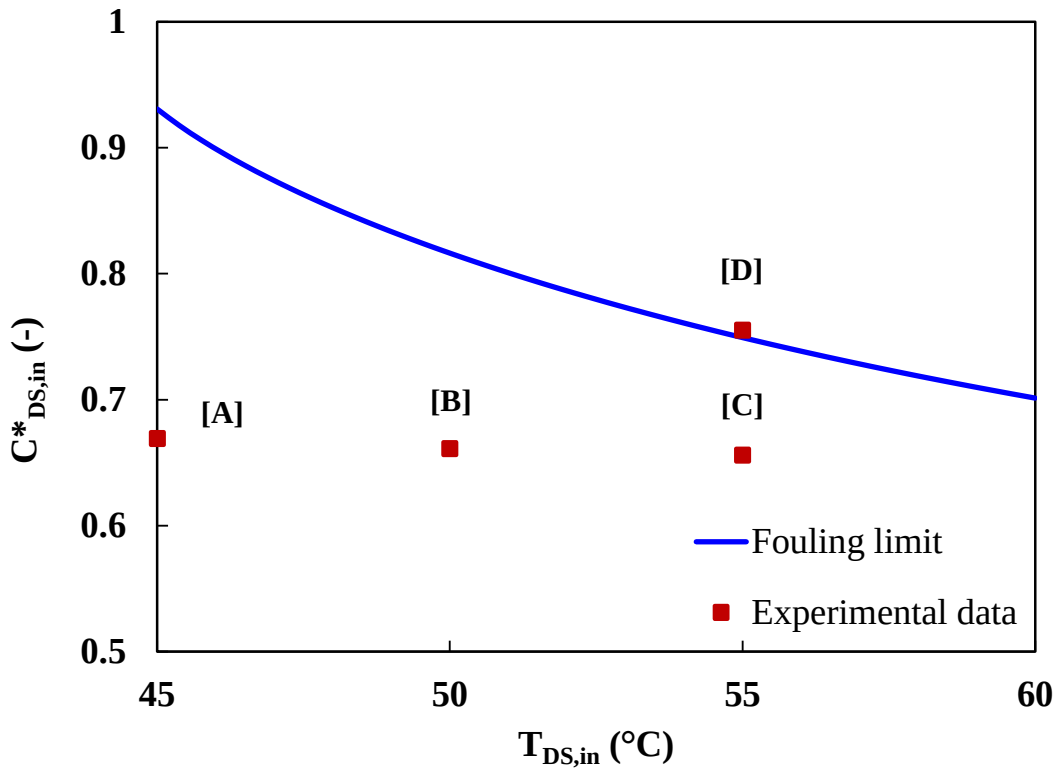

Figure 3.3. Comparison between theoretical fouling limit and experimental test conditions.

3.6 Results and discussion

The operation of LAMEE is challenging at high solution concentrations or near saturation due to the chance of crystal formation on/within the membrane pores. This section applies the model

presented in section 3.4.2 to determine (1) the fouling limits for three different desiccant solutions ($MgCl_2$(aq), $CaCl_2$(aq), and LiCl(aq)) for a range of design parameters and operating conditions and (2) the reduction in moisture transfer flux due to crystallization fouling for $MgCl_2$(aq) at various locations along the LAMEE. It should be mentioned that energy exchanger performance is also important. Changing a parameter that can reduce fouling, may also reduce performance. There may be some optimal selection for a given design or application.

3.6.1 Effect of solution temperature on fouling limits

LAMEEs may experience a wide range of temperatures depending on the process in its application. For example, during the regeneration process, temperature can be around 40 to 50°C [88]. Figures 3.4 to 3.6 present the limits of crystallization fouling as a function of solution inlet temperature. In these figures, any point above the line of inlet air relative humidity, leads to saturation at the membrane surface and crystallization fouling is likely. On the other hand, saturation will not occur for the points below the relative humidity line and thus fouling is unlikely.

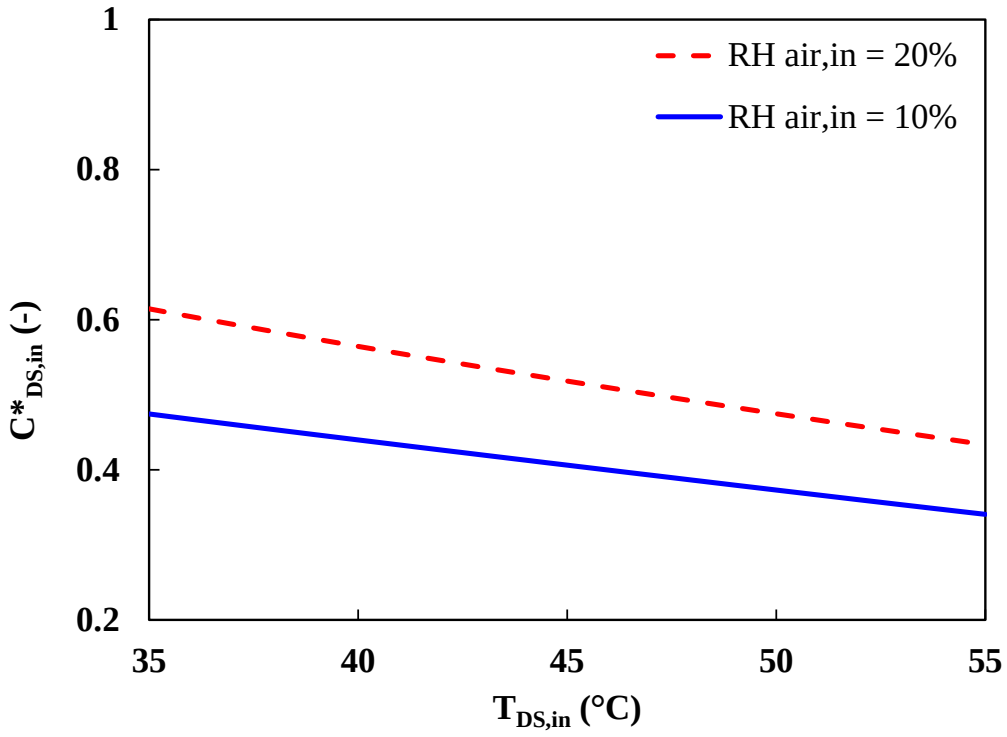

Figure 3.4. Fouling limits at LAMEE inlet for $MgCl_2$(aq) versus solution temperature at different $RH_{air,in}$ at Cr* = 4, NTU = 4, NTU_m = 3.3, $T_{air,in}$= 30°C.

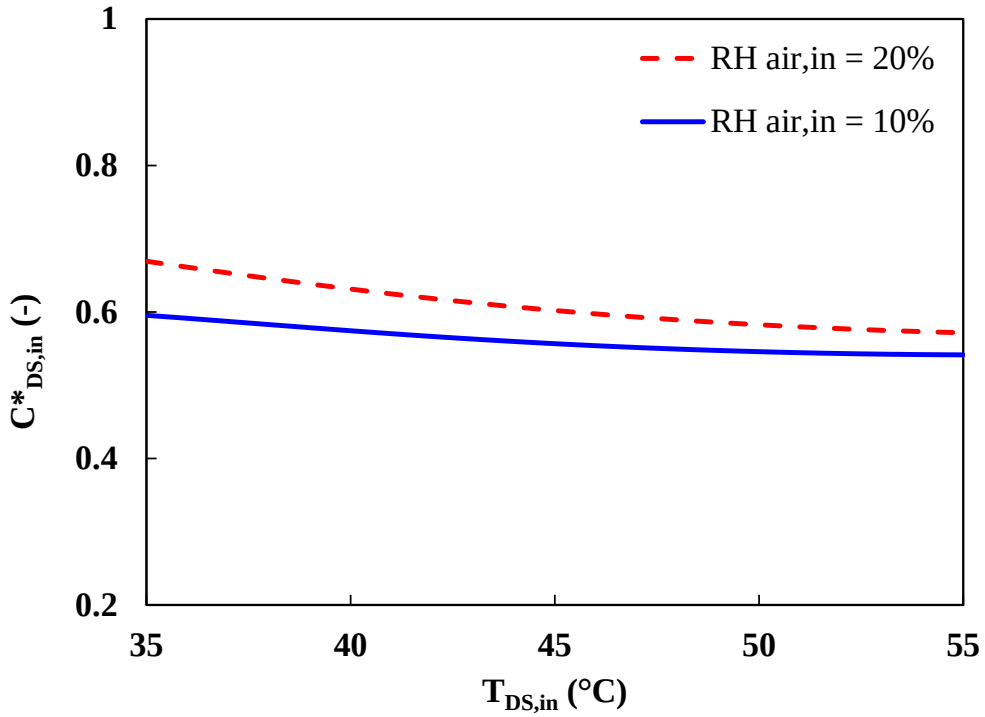

Figure 3.5. Fouling limits at LAMEE inlet for $CaCl_2$(aq) versus solution temperature at different $RH_{air,in}$ at Cr* = 4, NTU = 4, NTU_m = 3.3, $T_{air,in}$= 30°C.

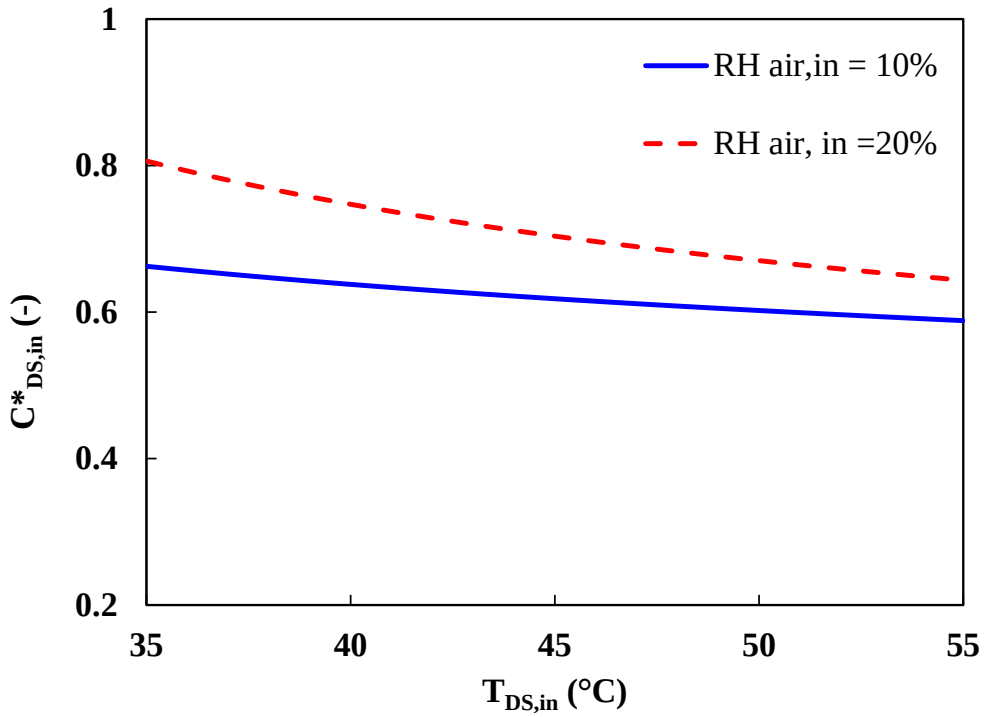

Figure 3.6. Fouling limits at LAMEE inlet for LiCl(aq) versus solution temperature at different $RH_{air,in}$ at Cr* = 4, NTU = 4, NTU_m = 3.3, $T_{air,in}$= 30°C.

As it can be seen in Figure 3.4, the allowable dimensionless solution concentration (C*) at the inlet decreases as the solution temperature increases indicating that LAMEEs are more susceptible to fouling at higher temperatures. Thus, highly concentrated solutions cannot be used at a higher solution temperature. A reason for it is that increasing the desiccant solution temperature results in a greater vapor pressure gradient through the membrane increasing the moisture transfer rate through the membrane increases. Therefore, concentration polarization increases on the membrane surface accelerating the fouling rate. The experimental results of fouling in a membrane distillation process working with NaCl(aq) also showed that an increase in the feed temperature leads to an increase in growth rate of crystals on the membrane surface [89]. The results in Figure 3.6 also agree with the results of Ref. [32] when the discrepancy between the experiment and model increased as the solution temperature increased, indicating a higher fouling rate at higher solution temperatures, as shown in Figure 3.7. In this figure, latent effectiveness is because of moisture transfer in the energy exchanger which is defined as the ratio of latent energy transferred in the system to the maximum possible latent energy transfer in the exchanger.

As shown in Figures 3.4 to 3.6, the gap between the fouling limit lines is larger at lower solution temperatures implying that by increasing temperature to high values the allowable $C^*_{DS,in}$ may reach to nearly a constant value regardless of inlet air relative humidity. For instance, the difference between $C^*_{DS,in}$ at $T_{DS,in}$ = 35°C for $MgCl_2$(aq) is about 28% while at $T_{DS,in}$ = 55°C is around 20%. Figures 3.4 to 3.6 also reveal that when the inlet air relative humidity increases, the allowable $C^*_{DS,in}$ also increases. The main reason is that at higher inlet air relative humidity, there is a lower vapor pressure gradient across the membrane resulting in lower supersaturation on the membrane surface and consequently the LAMEE can work at high concentrations without fouling.

Figure 3.8 shows a comparison of dimensionless solution concentration at the inlet ($C^*_{DS,in}$) for the studied desiccant solutions when the solution temperature varies from 35 to 55°C. It is observed from the figure that the lowest C* values correspond to $MgCl_2$(aq). As a result, $MgCl_2$(aq) is more susceptible to crystallization fouling followed by $CaCl_2$(aq) and LiCl(aq). The study of Afshin et al. [84] in run-around membrane energy exchangers also showed that $MgCl_2$(aq) is the most susceptible desiccant solution to crystal formation. Thus, it is recommended to check the fouling limits of $MgCl_2$(aq) before employing it in LAMEE to avoid the performance deterioration due to the fouling.

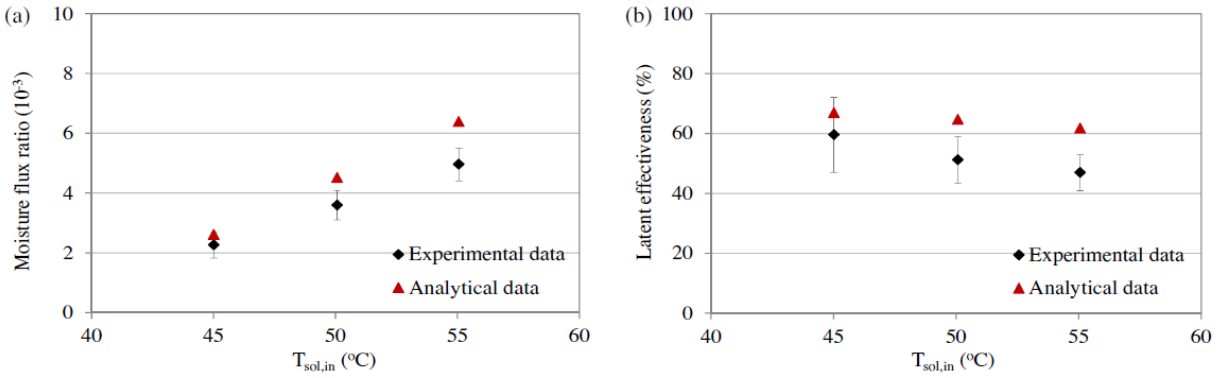

Figure 3.7. Effect of inlet temperature of desiccant solution on regeneration (a) moisture flux ratio and (b) latent effectiveness (extracted from Ref. [32]).

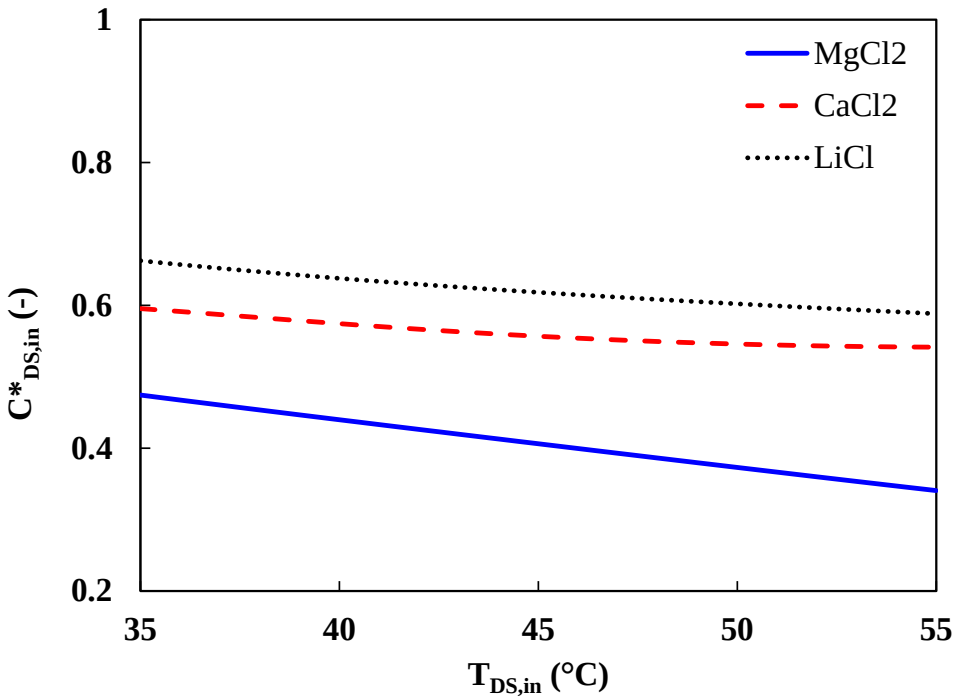

Figure 3.8. Comparison of fouling limits for $MgCl_2$(aq), $CaCl_2$(aq), and LiCl(aq) as a function of solution temperature at $RH_{air,in}$ =10%, Cr* = 4, NTU = 4, NTU_m = 3.3, $T_{air,in}$= 30°C.

3.6.2 Effect of Cr* on fouling limits

In addition to solution temperature, hydrodynamics is another important parameter in LAMEE performance. Figure 3.9 shows the effect of Cr* on the fouling limits for the three desiccant solutions. The inlet solution and air temperature are kept constant at 55°C and 30°C, respectively in Figure 3.9.

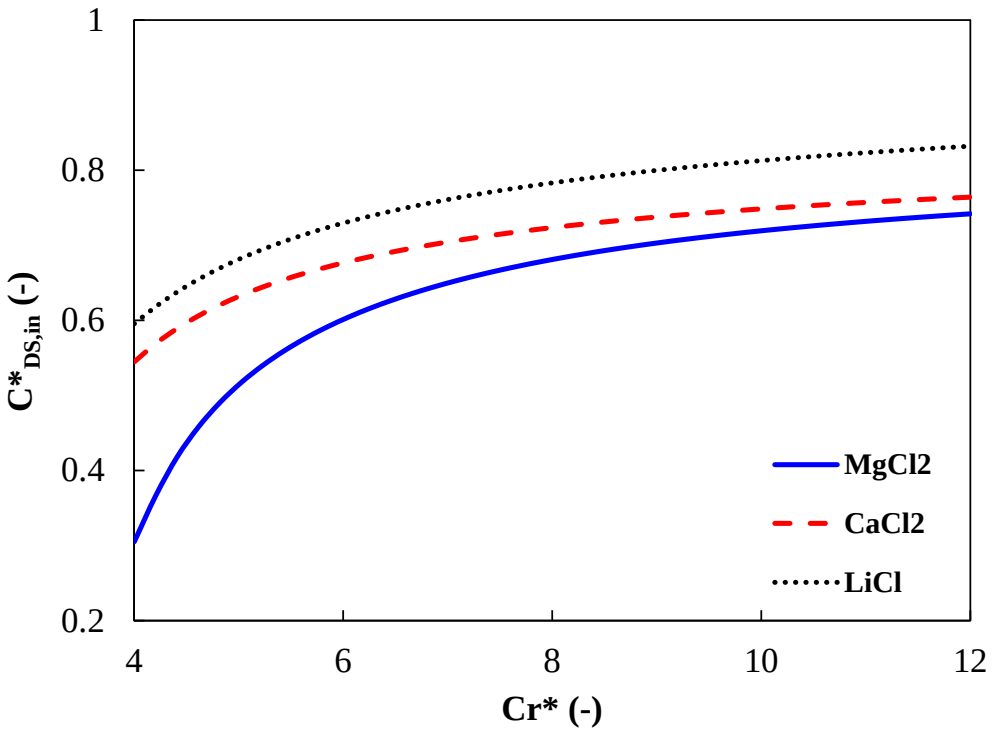

Figure 3.9. Fouling limits at LAMEE inlet for three desiccant solutions versus Cr* at $RH_{air,in}$ =10%, $T_{air,in}$ = 30°C, $T_{DS,in}$ = 55°C, NTU = 4, NTU_m = 3.3.

Figure 3.9 shows that the dimensionless solution concentration at the inlet ($C^*_{DS,in}$) increases when Cr* is increased. The reason is that as the mass flow rate increases more moisture needs to be removed before the solution becomes saturated. Doubling the desiccant solution mass flow rate ($\dot{m}_{DS}$) means the moisture transfer flux through the membrane ($\dot{m}''_c$) needs to double to reach saturation. Doubling $\dot{m}_{DS}$ increases $\dot{m}''_c$ but the increase in $\dot{m}''_c$ will be less than 2 times. Therefore, increasing $\dot{m}_{DS}$ decreases the risk of fouling. Increasing $\dot{m}_{DS}$ would also increase shear stress at the membrane surface and increase removal of foulants which is not included in the current model.

Figure 3.9 also shows that the range of variations in $C^*_{DS,in}$ for $MgCl_2$(aq) is greater than the other two desiccant solutions. Changing Cr* from 4 to 12 changes $C^*_{DS,in}$ nearly 2 times for $MgCl_2$(aq), while the amount of change for both $CaCl_2$(aq) and LiCl(aq) is about 40%. It can be concluded that when operating a LAMEE with $MgCl_2$(aq) at low Cr* value, the solution concentration at the inlet should be kept low to prevent crystallization fouling at the outlet.

3.6.3 Effect of NTU_m on fouling limits

Another parameter that plays a role on LAMEE performance and fouling formation is number of mass transfer units (NTU_m). This section discusses the effect of vapor diffusion resistance (VDR) of the membrane which can change NTU_m and consequently affect the fouling limits. The inlet temperature of desiccant solution and air are kept constant at 55°C and 35°C, respectively while the membrane VDR varies from 1 to 200 s/m which corresponds to NTU_m values of 4.1 to 1.2 at NTU = 4.

Figure 3.10 presents the effect of changing NTU_m on fouling limits of the three desiccant solutions. Any point above the fouling limit line is prone to supersaturation and thus crystallization fouling is likely. As mentioned in Chapter 2 and also reported in Ref [24], the lower the VDR, the higher the NTU_m and the higher the moisture transfer rate through the membrane. Figure 3.10 shows that as NTU_m increases (i.e., as the VDR of the membrane decreases), the tendency to crystal formation increases. Hence, the risk of crystallization fouling increases at elevated NTU_m (lower VDR).

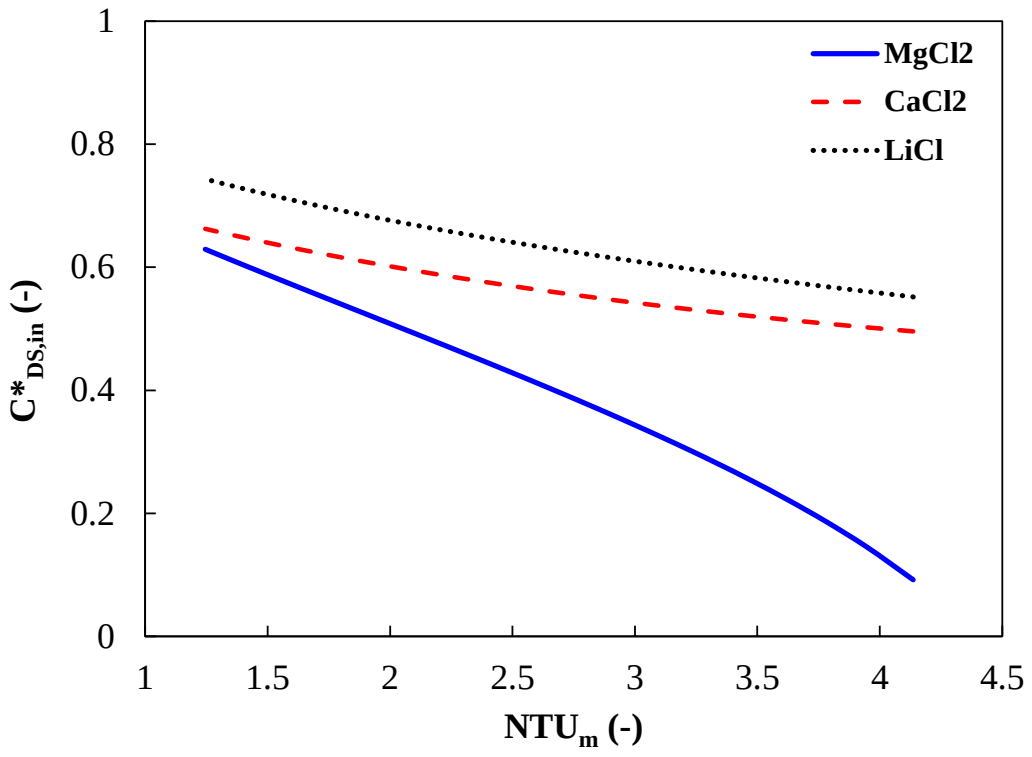

Figure 3.10. Fouling limits at LAMEE inlet for three desiccant solutions versus NTU_m at $RH_{air,in}$ =10%, $T_{air,in}$ = 30°C, $T_{DS,in}$ = 55°C, Cr* = 4, NTU = 4.

When NTU_m changes from 4.1 to 1.2, $C^*_{DS,in}$ changes more drastically for $MgCl_2$(aq) (~90%) compared to $CaCl_2$(aq) and LiCl(aq) which are about 25% for both. Hence, it is suggested to use $CaCl_2$(aq) or LiCl(aq) at higher values of NTU_m since they have less susceptibility to fouling. It is desirable to have a lower VDR in a LAMEE, but choosing a small VDR increases the risk of fouling. At some point it might be counterproductive to invest on a high performing membrane (low VDR) because fouling may negate any performance gains.

3.6.4 Variations of moisture transfer flux for $MgCl_2$(aq)

This section discusses the reduction in moisture transfer flux due to fouling as a function of membrane length for a LAMEE operating with $MgCl_2$(aq). Once the inlet operating conditions are given (which are selected from the graphs mentioned above that leads to fouling), the normalized moisture transfer flux is calculated using Eq. (3.21) to (3.23).

Figure 3.11 shows the variations of normalized moisture transfer flux (M*) against membrane location at $RH_{air,in}$ = 10% for two different inlet solution concentrations after 6 hours of operation. The decline in M* at $C^*_{DS,in}$ = 0.8 and $C^*_{DS,in}$ = 0.85 are about 2% and 20%, respectively. As the solution concentration increases, the supersaturation at the solution-membrane interface rises which leads to greater rate of crystallization fouling. As a result, higher degrees of supersaturation lead to severe crystal formation/growth and therefore the decline in moisture transfer is more significant. Moreover, it can be observed that at $C^*_{DS,in}$ = 0.8, M* starts to decline at further point on the membrane compared to the solution with $C^*_{DS,in}$ = 0.85 because saturation conditions start to emerge earlier for higher solution concentrations.

Figure 3.12 shows M* versus the length of membrane for two different times at $C^*_{DS,in}$ = 0.85 and $RH_{air,in}$ = 10%. After 6 hours of operation, the decline in M* is about 20%, while after 12 hours the decline in M* is nearly 35%. As mentioned in Chapter 2, the growth of crystal particles covers a larger area of the membrane surface in the course of time which decelerates the moisture transfer flux through the membrane.

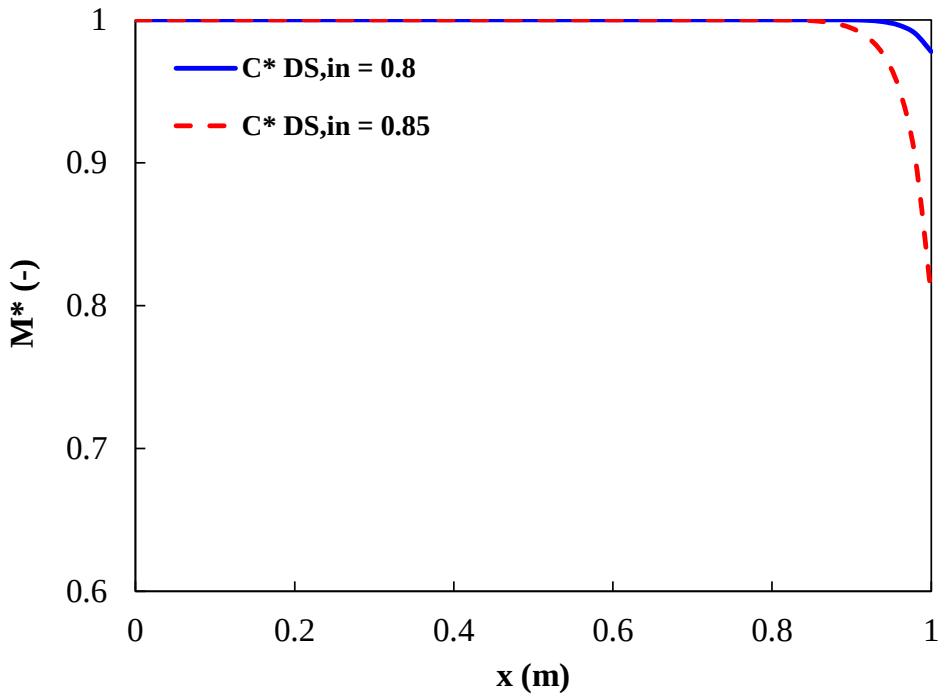

Figure 3.11. Variations of normalized moisture transfer flux versus membrane location for two solution concentrations at $RH_{air,in}$ = 10%, $T_{air,in}$ = 30°C, $T_{DS,in}$ = 35°C, Cr* = 4, NTU = 4.

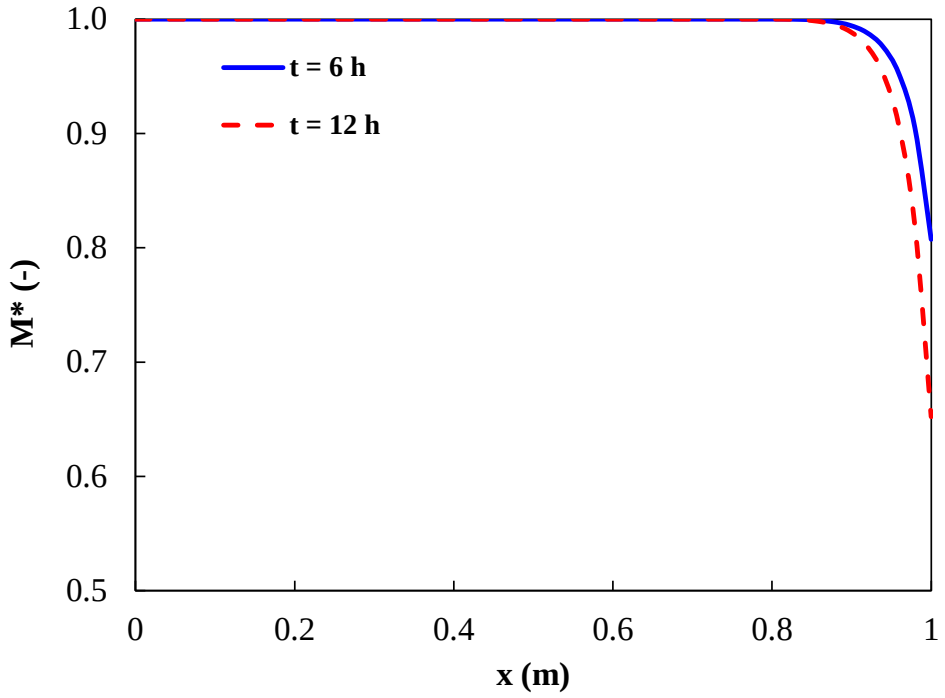

Figure 3.12. Variations of normalized moisture transfer flux versus membrane length for two different times at $C^*_{DS,in}$ = 0.85, $RH_{air,in}$ = 10%, $T_{air,in}$ = 30°C, $T_{DS,in}$ = 35°C, Cr* = 4, NTU = 4.

Figure 3.13 presents the variations of M* as a function of membrane length after 6 hours for two different Cr* values. Increasing Cr* from 4 to 5 has a remarkable effect on M* (only 1% decline in M* at Cr* = 5 and 20% decline in M* at Cr* = 4). As explained in section 3.2, increasing Cr* results in more moisture removal before the solution becomes saturated and therefore the risk of crystallization fouling increases.

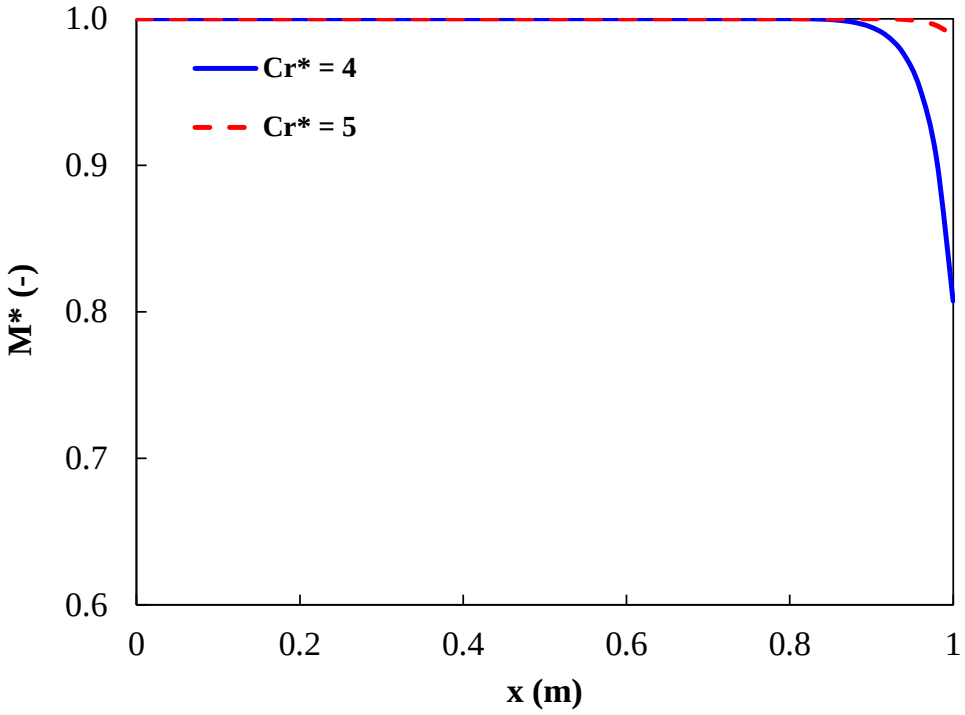

Figure 3.13. Variations of M* versus membrane location after 6 hours for two different Cr* values at $C^*_{DS,in}$ = 0.85, $RH_{air,in}$ = 10%, $T_{air,in}$ = 30°C, $T_{DS,in}$ = 35°C, and NTU = 4.

3.7 Conclusions

In this chapter, a theoretical model was developed to predict the crystallization fouling limits of a counter-flow LAMEE for a range of operational and design factors. In addition, based on the semi-empirical model developed in previous chapter, the variations of normalized moisture transfer flux due to fouling was estimated for a LAMEE working with $MgCl_2$(aq). The significant conclusions of this chapter are listed below.

1- According to the fouling limit model, as the solution temperature at the LAMEE inlet increases, the susceptibility to fouling increases.

2- Among the studied desiccant solutions in this chapter, the risk of crystallization fouling is highest for $MgCl_2$(aq) followed by $CaCl_2$(aq) and LiCl(aq).
3- Increasing the heat capacity ratio reduces the risk of crystallization fouling because when the solution mass flow rate increases more moisture has to be removed before the solution is saturated.
4- As the vapor diffusion resistance of the membrane decreases (i.e., the number of mass transfer units (NTU_m) increase) the risk of crystallization fouling increases.
5- Once the desiccant solution concentration at the inlet of the LAMEE increases, the solution becomes supersaturated earlier along the membrane length and consequently the decline in moisture transfer rate is greater.

CHAPTER 4

SUMMARY, CONCLUSIONS, AND FUTURE WORK

This chapter contains a summary of the thesis, the significant conclusions of the thesis and provides some recommendations for future research work.

4.1 Summary

The main goal of this thesis was to develop a model to determine the crystallization fouling rates and the crystallization fouling limits in LAMEEs. To meet these goals, the following objectives were addressed: (i) develop and validate a predictive model for determining the moisture transfer rate in LAMEEs due to crystallization fouling, and (ii) quantify the impact of design and operating conditions on crystallization fouling in LAMEEs.

In Chapter 2, a semi-empirical model was developed to determine the decline in moisture transfer flux due to fouling and the fouling rate in a LAMEE with a stagnant solution. The model was based on determining the solution concentration at the membrane surface and then using the surface blockage of the membrane to estimate the decline in moisture transfer rate. The model was verified with the experimental data available in the literature and was used to predict the effect of operating and design conditions on the fouling rate. Moreover, it was used to predict the time when the moisture transfer flux due to fouling declines to a specific value.

In Chapter 3, the model in Chapter 2 was expanded to apply to a flowing solution in a counter-flow LAMEE. The model was developed to determine the design and operating condition that would initiate fouling. Fouling is firs possible (i.e., the fouling limit) when the concentration of the aqueous salt solution reaches saturation at the solution-membrane interface, which may trigger the formation and growth of crystals. The fouling limits were shown for three desiccant solutions for a counter-flow LAMEE at various operating and design conditions. Also, the reduction in moisture transfer flux through the membrane was predicted for a LAMEE working with magnesium chloride.

4.2 Conclusions

It can be concluded that the formation and growth of crystals on the membrane impedes the water vapor transfer through the membrane pores and consequently over time moisture transfer flux

decreases. Based on a sensitivity analysis in this thesis, the convective mass transfer coefficient of air has the greatest effect on both moisture transfer rate and fouling rate. On the other hand, the fouling rate constant of crystallization and vapor diffusion resistance of the membrane have the lowest influence on the moisture transfer rate and accordingly the fouling rate. The model predictions showed that reducing the vapor diffusion resistance of the membrane and increasing the solution concentration increases the required cleaning frequency.

The fouling limit model showed that increasing the solution temperature at LAMEE inlet increases the risk of fouling. Among the studied desiccant solutions, magnesium chloride solution is the most susceptible liquid desiccant to fouling followed by calcium chloride and lithium chloride. The results revealed that increasing the solution mass flow rate results in more removal of moisture before the solution is saturated and therefore the likelihood of fouling reduces. It was also shown that decreasing the vapor diffusion resistance of the membrane increases the risk of fouling. Besides, the results showed that an increase in solution concentration at LAMEE inlet causes formation/growth of crystals at closer points along the membrane and the reduction in moisture transfer flux is more significant.

4.3 Recommendations for future work

Some recommendations for future research are listed below:

- The model developed in this thesis was based on the experimental data for isothermal conditions and then was used to approximate the fouling for non-isothermal conditions. It is suggested to conduct fouling experiments for non-isothermal conditions and validate the model at these conditions to increase confidence in the predicted results and non-isothermal conditions.
- It is recommended that the reaction kinetics of crystallization and temperature dependence of chemical reaction on the membrane are considered in the model.
- The fouling model in this thesis was developed for $MgCl_2$ that can be extended to other desiccants by finding the empirical values from the experiments (i.e., the fouling rate constant). Thus, it is recommended to develop a model for other desiccant solutions and perform experiments to validate the results.

- The fouling limits model for a flowing solution was developed for a counter-flow LAMEE. It is suggested to study fouling limits for the co-current flow and compare the results with the counter-current flow.
- It is suggested to develop a computational fluid dynamic (CFD) model to predict the reduction of moisture transfer rate due to fouling in LAMEEs. CFD simulations enable more detailed field variables on the solution side such as shear stress which may cause fouling removal.

REFERENCES

[1] T.R. Bott, Fouling of heat exchangers, first ed., Elsevier Science, 1995.

[2] P.S. Goh, W.J. Lau, M.H.D. Othman, A.F. Ismail, Membrane fouling in desalination and its mitigation strategies, Desalination 425 (2018) 130–155.

[3] H. Müller-Steinhagen, Heat transfer fouling: 50 years after the Kern and Seaton model, Heat Transfer Engineering 32 (2011) 1–13.

[4] S. Shirazi, C.-J. Lin, D. Chen, Inorganic fouling of pressure-driven membrane processes – A critical review, Desalination 250 (1) (2010) 236–248.

[5] H. Müller-Steinhagen, M.R. Malayeri, A.P. Watkinson, Heat exchanger fouling: Mitigation and cleaning strategies, Heat Transfer Engineering 32 (3–4) (2011) 189–196.

[6] L. Pérez-Lombard, J. Ortiz, C. Pout, A review on buildings energy consumption information, Energy and Buildings 40 (2008) 394–398.

[7] H.V. Inamdar, E.A. Groll, J.A. Weibel, S.V. Garimella, Prediction of air-side particulate fouling of HVAC&R heat exchangers, Applied Thermal Engineering 104 (2016) 720– 733.

[8] C. Shen, Y. Wang, Z. Zhao, Y. Jiang, Y. Yao, Decoupling analysis on the variations of liquid velocity and heat flux in the test of fouling thermal resistance, International Journal of Heat and Mass Transfer 123 (2018) 227–238.

[9] I.H. Bell, E.A. Groll, Air-side particulate fouling of microchannel heat exchangers: Experimental comparison of air-side pressure drop and heat transfer with plate-fin heat exchanger, Applied Thermal Engineering 31 (5) (2011) 742–749.

[10] C. Zhang, Z. Tang, Z. Zhang, J. Shi, J. Chen, M. Zhang, Impact of airside fouling on microchannel heat exchangers, Applied Thermal Engineering 128 (2018) 42–50.

[11] S. Wright, G. Andrews, H. Sabir, A review of heat exchanger fouling in the context of aircraft air-conditioning systems, and the potential for electrostatic filtering, Applied Thermal Engineering 29 (13) (2009) 2596–2609.

[12] S. Lopata, P. Oclon, Numerical study of the effect of fouling on local heat transfer conditions in a high-temperature fin-and-tube heat exchanger, Energy 92 (1) (2015) 100–

116.

[13] M.E. Walker, I. Safari, R.B. Theregowda, M.-K. Hsieh, J. Abbasian, H. Arastoopour, D.A. Dzombak, D.C. Miller, Economic impact of condenser fouling in existing thermoelectric power plants, Energy 44 (1) (2012) 429–437.

[14] B.A. Qureshi, S.M. Zubair, The impact of fouling on the condenser of a vapor compression refrigeration system: An experimental observation, International Journal of Refrigeration 38 (2014) 260–266.

[15] R. Zhang, T. Hong, Modeling of HVAC operational faults in building performance simulation, Applied Energy 202 (2017) 178–188.

[16] H. Cheung, K. Shan, S. Wang, A fault-tolerant control method of balancing valves for condenser fouling in water-cooled chillers, Energy Procedia 142 (2017) 1793–1798.

[17] M.R. Jalalirad, M.S. Abd-Elhady, M.R. Malayeri, Cleaning action of spherical projectiles in tubular heat exchangers, International Journal of Heat and Mass Transfer 57 (2) (2012) 491–499.

[18] R.S. Mohamed, S. Kandil, Y. Wang, J.J. McArthur, Fault detection for non-condensing boilers using simulated building automation system sensor data, Advanced Engineering Informatics 46 (2020) 101176.

[19] B.A. Qureshi, S.M. Zubair, A complete model of wet cooling towers with fouling in fills, Applied Thermal Engineering 26 (2006) 1982–1989.

[20] R. Gao, C. Shen, X. Wang, Y. Yao, A generalized prediction model of waterside fouling for internally enhanced tubes in shell and tube condensers, Applied Thermal Engineering 195 (2021) 117150.

[21] N.T. Charles, D.W. Johnson, The occurrence and characterization of fouling during membrane evaporative cooling, Journal of Membrane Science 319 (1–2) (2008) 44–53.

[22] R. Crawford, A.K. Da Silva, Experimental testing of a passive, evaporation-based roof cooling system, Energy and Buildings 71 (2014) 12–19.

[23] A.O. Olufade, C.J. Simonson, Detection of crystallization fouling in a liquid-to-air

membrane energy exchanger, Experimental and Thermal Fluid Science 92 (2018) 33–45.

[24] A.O. Olufade, C.J. Simonson, Application of indirect non-invasive methods to detect the onset of crystallization fouling in a liquid-to-air membrane energy exchanger, International Journal of Heat and Mass Transfer 127 (2018) 663–673.

[25] A.O. Olufade, C.J. Simonson, Calibration of indirect methods to detect the onset of fouling in a liquid-to-air membrane energy exchanger, International Journal of Heat and Mass Transfer 151 (2020) 118885.

[26] A.O. Olufade, C.J. Simonson, Characterization of the Evolution of Crystallization Fouling in Membranes, ACS Omega 3 (12) (2018) 17188–17198.

[27] B. Xing, Experimental detection and reversal of crystallization fouling in a liquid-to-air membrane energy exchanger, M.Sc. Thesis, University of Saskatchewan, SK, 2020.

[28] G. Ge, M.R.H. Abdel-Salam, R.W. Besant, C.J. Simonson, Research and applications of liquid-to-air membrane energy exchangers in building HVAC systems at University of Saskatchewan: A review, Renewable and Sustainable Energy Reviews 26 (2013) 464–479.

[29] B. Erb, Run-around membrane energy exchanger performance and operational control strategies, M.Sc. Thesis, University of Saskatchewan, Saskatoon, SK, Canada, 2009.

[30] M.R.H. Abdel-Salam, G. Ge, M. Fauchoux, R.W. Besant, C.J. Simonson, State-of-the-art in liquid-to-air membrane energy exchangers (LAMEEs): A comprehensive review, Renewable and Sustainable Energy Reviews 39 (2014) 700–728.

[31] A.H. Abdel-Salam, C.J. Simonson, Annual evaluation of energy, environmental and economic performances of a membrane liquid desiccant air conditioning system with/without ERV, Applied Energy 116 (2014) 134–148.

[32] G. Ge, D. Ghadiri Moghaddam, A.H. Abdel-Salam, R.W. Besant, C.J. Simonson, Comparison of experimental data and a model for heat and mass transfer performance of a liquid-to-air membrane energy exchanger (LAMEE) when used for air dehumidification and salt solution regeneration, International Journal of Heat and Mass Transfer 68 (2014) 119–131.

[33] M.R.H. Abdel-Salam, R.W. Besant, C.J. Simonson, Sensitivity of the performance of a flat-plate liquid-to-air membrane energy exchanger (LAMEE) to the air and solution channel widths and flow maldistribution, International Journal of Heat and Mass Transfer 84 (2015) 1082–1100.

[34] D. Ghadiri Moghaddam, P. LePoudre, G. Ge, R.W. Besant, C.J. Simonson, Small-scale single-panel liquid-to-air membrane energy exchanger (LAMEE) test facility development, commissioning and evaluating the steady-state performance, Energy and Buildings 66 (2013) 424–436.

[35] B. Bansal, X.D. Chen, H. Muller-Steinhagen, Analysis of 'classical' deposition rate law for crystallization fouling, Chemical Engineering and Processing: Process Intensification 47 (2008) 1201–1210.

[36] A. Al-Janabi, M.R. Malayeri, Innovative non-metal heat transfer surfaces to mitigate crystallization fouling, International Journal of Thermal Sciences 138 (2019) 384–392.

[37] Y. Lv, K. Lu, Y. Ren, Composite crystallization fouling characteristics of normal solubility salt in double-pipe heat exchanger, International Journal of Heat and Mass Transfer 156 (2020) 119883.

[38] The World Bank Group, GDP (current US$) – United States, 2019, https://data.worldbank.org/indicator/NY.GDP.MKTP.CD?locations=US.

[39] The World Bank Group, GDP (current US$) – European Union, 2019, https://data.worldbank.org/indicator/NY.GDP.MKTP.CD?locations=EU.

[40] The World Bank Group, GDP (current US$) – Canada, 2019, https://data.worldbank.org/indicator/NY.GDP.MKTP.CD?locations=CA.

[41] A.H. Abdel-Salam, G. Ge, C.J. Simonson, Performance analysis of a membrane liquid desiccant air-conditioning system, Energy and Buildings 62 (2013) 559–569.

[42] C. Shen, C. Cirone, X. Wang, A method for developing a prediction model of water-side fouling on enhanced tubes, International Journal of Heat and Mass Transfer 85 (2015) 336–342.

[43] L. Cremaschi, J.D. Spitler, E. Lim, A. Ramesh, Waterside fouling performance in brazed-plate-type condensers for cooling tower applications, HVAC&R Research 17 (2) (2011) 198–217.

[44] C. Shen, C. Cirone, A.M. Jacobi, X. Wang, Fouling of enhanced tubes for condensers used in cooling tower systems: A literature review, Applied Thermal Engineering 79 (2015) 74–87.

[45] B.A. Qureshi, S.M. Zubair, Predicting the impact of heat exchanger fouling in refrigeration systems, International Journal of Refrigeration 44 (2014) 116–124.

[46] X. Zhao, M. Yang, H. Li, A virtual condenser fouling sensor for chillers, Energy and Buildings 52 (2012) 68–76.

[47] J. Woods, Membrane processes for heating, ventilation, and air conditioning, Reneweable and Sustainable Energy Reviews 33 (2014) 290–304.

[48] X. Liu, M. Qu, X. Liu, L. Wang, J. Warner, Numerical modeling and performance analysis of a membrane-based air dehumidifier using ionic liquid desiccant, Applied Thermal Engineering 175 (2020) 115395.

[49] L.D. Tijing, Y.C. Woo, J.S. Choi, S. Lee, S.H. Kim, H.K. Shon, Fouling and its control in membrane distillation-A review, Journal of Membrane Science 475 (2015) 215–244.

[50] D.M. Warsinger, J. Swaminathan, E. Guillen-Burrieza, H.A. Arafat, J.H. Lienhard V, Scaling and fouling in membrane distillation for desalination applications: A review, Desalination 356 (2015) 294–313.

[51] D. González, J. Amigo, F. Suárez, Membrane distillation: Perspectives for sustainable and improved desalination, Reneweable and Sustainable Energy Reviews 80 (2017) 238–259.

[52] T. Tong, A.F. Wallace, S. Zhao, Z. Wang, Mineral scaling in membrane desalination: Mechanisms, mitigation strategies, and feasibility of scaling-resistant membranes, Journal of Membrane Science 579 (2019) 52–69.

[53] D.M. Warsinger, E.W. Tow, J. Swaminathan, J.H. Lienhard V, Theoretical framework for predicting inorganic fouling in membrane distillation and experimental validation with

calcium sulfate, Journal of Membrane Science 528 (2017) 381–390.

[54] M. Ramezanianpour, M. Sivakumar, An analytical flux decline model for membrane distillation, Desalination 345 (2014) 1–12.

[55] H. Julian, B. Lian, H. Li, X. Liu, Y. Wang, G. Leslie, V. Chen, Numerical study of CaCO3 scaling in submerged vacuum membrane distillation and crystallization (VMDC), Journal of Membrane Science 559 (2018) 87–97.

[56] H. Cho, Y. Choi, S. Lee, J. Sohn, J. Koo, Membrane distillation of high salinity wastewater from shale gas extraction: effect of antiscalants, Desalination and Water Treatment 57 (55) (2016) 26718–26729.

[57] J.S. Cho, H. Kim, J.S. Choi, S. Lee, T.M. Hwang, H. Oh, D. Ryook, J.H. kim, Prediction of reverse osmosis membrane fouling due to scale formation in the presence of dissolved organic matters using genetic programming, Desalination and Water Treatment 15 (1–3) (2010) 121–128.

[58] H.J. Oh, Y.K. Choung, S. Lee, J.S. Choi, T.M. Hwang, J.H. Kim, Scale formation in reverse osmosis desalination: model development, Desalination 238 (1–3) (2009) 333–346.

[59] M. Shmulevsky, X. Li, H. Shemer, D. Hasson, R. Semiat, Analysis of the onset of calcium sulfate scaling on RO membranes, Journal of Membrane Science 524 (2017) 299–304.

[60] T.R. Bott, Aspects of crystallization fouling, Experimental Thermal and Fluid Science 14 (4) (1997) 356–360.

[61] M.G. Mwaba, M.R. Golriz, J. Gu, A semi-empirical correlation for crystallization fouling on heat exchange surfaces, Applied Thermal Engineering 26 (4) (2006) 440–447.

[62] T.M. Pääkkönen, M. Riihimäki, C.J. Simonson, E. Muurinen, R. L. Keiski, Modeling CaCO3 crystallization fouling on a heat exchanger surface - Definition of fouling layer properties and model parameters, International Journal of Heat and Mass Transfer 83 (2015) 84–98.

[63] J. Gilron, D. Hasson, Calcium sulphate fouling of reverse osmosis membranes: Flux decline mechanism, Chemical Engineering Science 42 (10) (1987) 2351–2360.

[64] D.Q. Kern, R.E. Seaton, A theoretical analysis of thermal surface fouling, British Chemical Engineering 4 (5) (1959) 258–262.

[65] M.S. Abd-Elhady, M.R. Malayeri, M.R. Jalalirad, Intensification of the cleaning action of structurally different projectiles by multiple injections and changing injection rate, Desalination 337 (1) (2014) 52–59.

[66] S. Lee, C.H. Lee, Effect of operating conditions on CaSO4 scale formation mechanism in nanofiltration for water softening, Water Research 34 (15) (2000) 3854–3866.

[67] S.H. Najibi, H. Müller-Steinhagen, M. Jamialahmadi, Calcium sulphate scale formation during subcooled flow boiling, Chemical Engineering Science 52 (8) (1997) 1265–1284.

[68] F. Brahim, W. Augustin, M. Bohnet, Numerical simulation of the fouling process, International Journal of Thermal Sciences 42 (3) (2003) 323–334.

[69] H.B. Hemingson, C.J. Simonson, R.W. Besant, Steady-state performance of a run-around membrane energy exchanger (RAMEE) for a range of outdoor air conditions, International Journal of Heat and Mass Transfer 54 (9–10) (2011) 1814–1824.

[70] ASHRAE Handbook-Fundamentals, Atlanta, GA, USA: ASHRAE, 2017.

[71] I. Hitsov, T. Maere, K. De Sitter, C. Dotremont, I. Nopens, Modelling approaches in membrane distillation: A critical review, Seperation and Purification Technology 142 (2015) 48–64.

[72] R.N. Goldberg, R.L. Nuttall, "Evaluated activity and osmotic coefficients for aqueous solutions: The alkaline earth metal halides, Journal of Physical and Chemical Reference Data 7 (1) (1978) 263–310.

[73] C.H. Tan, H.Y. Ng, Revised external and internal concentration polarization models to improve flux prediction in forward osmosis process, Desalination 309 (2013) 125–140.

[74] P. Navid, S. Niroomand, C.J. Simonson, A New Approach to Delay or Prevent Frost Formation in Membranes, Journal of Heat Transfer 141 (1) (2019) 1–11.

[75] L.Z. Zhang, Y. Jiang, Y.P. Zhang, Membrane-based humidity pump: Performance and limitations, Journal of Membrane Science 171 (2) (2000) 207–216.

[76] ASME/ANSI, Performance Test Code 19.1 Test Uncertainty: Instruments and Apparatus, New York, 1998.

[77] C.R. Iskra, C.J. Simonson, Convective mass transfer coefficient for a hydrodynamically developed airflow in a short rectangular duct, International Journal of Heat and Mass Transf 50 (11–12) (2007) 2376–2393.

[78] D. Ghadiri Moghaddam, A. Oghabi, G. Ge, R.W. Besant, C.J. Simonson, Numerical model of a small-scale liquid-to-air membrane energy exchanger: Parametric study of membrane resistance and air side convective heat transfer coefficient, Applied Thermal Engineering 61 (2) (2013) 245–258.

[79] G. Guan, C. Yao, S. Lu, Y. Jiang, H. Yu, X. Yang, Sustainable operation of membrane distillation for hypersaline applications: Roles of brine salinity, membrane permeability and hydrodynamics, Desalination 445 (2018) 123–137.

[80] M.M. Derby, A.N. Adams, P.P. Chakraborty, M.R. Haque, R.A. Huber, J.A. Morrow, G.A. Riley, M. Ross, E.M. Stallbaumer, A.R. Betz, H. Bindra, Heat and Mass Transfer in the Food, Energy, and Water Nexus—A Review, Journal of Heat Transfer 142 (9) (2020) 090801-1-090801-32.

[81] N.A. Ahmad, P.S. Goh, L.T. Yogarathinam, A.K Zulhairun, A.F. Ismail, Current advances in membrane technologies for produced water desalination, Desalination 493 (2020) 114643.

[82] P.S. Goh, T. Matsuura, A.F. Ismail, N. Hilal, Recent trends in membranes and membrane processes for desalination, Desalination 391 (2016) 43–60.

[83] A. Gurubalan, C.J. Simonson, A comprehensive review of dehumidifiers and regenerators for liquid desiccant air conditioning system, Energy Conversion and Management 240 (2021) 114234.

[84] M. Afshin, C.J. Simonson, R.W. Besant, Crystallization Limits of LiCl-Water and $MgCl_2$-Water Salt Solutions as Operating Liquid Desiccant in the RAMEE System, Ashrae Transactions 116 (2010) 494–506.

[85] D. Ghadiri Moghaddam, M. Fauchoux, R.W. Besant, C.J. Simonson, Investigating

similarity between a small-scale liquid-to-air membrane energy exchanger (LAMEE) and a full-scale (100 L/s) LAMEE: Experimental and numerical results, International Journal of Heat and Mass Transfer 77 (2014) 464–474.

[86] M.J. Blandamer, J.B.F.N. Engberts, P.T. Gleeson, J.C.R. Reis, Activity of water in aqueous systems; A frequently neglected property, Chemical Society Reviews 34 (2005) 440–458.

[87] M. Afshin, Selection of the Liquid Desiccant in a Run-Around Membrane Energy Exchanger, M.Sc. Thesis, University of Saskatchewan, SK, 2010.

[88] G.A. Longo, A. Gasparella, Experimental and theoretical analysis of heat and mass transfer in a packed column dehumidifier/regenerator with liquid desiccant, International Journal of Heat and Mass Transfer 48 (2005) 5240–5254.

[89] F. Kiefer, A. Prabst, T. Sattelmayer, Membrane scaling in Vacuum Membrane Distillation – Part 2: Crystallization kinetics and process performance, Journal of Membrane Science 590 (2019) 117293.

APPENDIX A

COPYRIGHT PERMISSIONS

Appendix A includes the copyright permissions for the unpublished and co-authored manuscripts in this thesis. For all the manuscripts that are included in a thesis, the College of Graduate and Postdoctoral Studies (CGPS) requires a written request from the publisher, i.e., copyright holder (for published manuscripts) and from co-author(s) (for unpublished manuscripts). The permission for using the unpublished manuscripts in this thesis are documented in this appendix.

A.1. PERMISSION FOR MANUSCRIPT USED IN CHAPTER 2

The manuscript presented in Chapter 2 is unpublished and therefore a copyright permission is obtained from all the co-authors of the manuscript which is included below:

Copyright Permission Request Form

I prepared a manuscript titled "A model for predicting the effect of crystallization fouling on moisture transfer in membrane energy exchangers" to be published as the second chapter of my M.Sc. thesis and submitted to the Department of Mechanical Engineering at the University of Saskatchewan. The authors who contributed to this manuscript are
Alireza Razmavar, Gurubalan Annadurai, Adesola Olufade, and Carey J. Simonson
I am requesting the permission to use the contents of this manuscript of my M.Sc. thesis and all subsequent revisions that may be prepared at the University of Saskatchewan. Please indicate your agreement by signing below:

Sincerely,
Alireza Razmavar
October 1, 2021

Permission granted by: Gurubalan Annadurai
Signature:
Date:

Copyright Permission Request Form

I prepared a manuscript titled “A model for predicting the effect of crystallization fouling on moisture transfer in membrane energy exchangers” to be published as the second chapter of my M.Sc. thesis and submitted to the Department of Mechanical Engineering at the University of Saskatchewan. The authors who contributed to this manuscript are

Alireza Razmavar, Gurubalan Annadurai, Adesola Olufade, and Carey J. Simonson

I am requesting the permission to use the contents of this manuscript of my M.Sc. thesis and all subsequent revisions that may be prepared at the University of Saskatchewan. Please indicate your agreement by signing below:

Sincerely,

Alireza Razmavar

October 1, 2021

Permission granted by: Adesola Olufade

Signature:

Date:

Copyright Permission Request Form

I prepared a manuscript titled "A model for predicting the effect of crystallization fouling on moisture transfer in membrane energy exchangers" to be published as the second chapter of my M.Sc. thesis and submitted to the Department of Mechanical Engineering at the University of Saskatchewan. The authors who contributed to this manuscript are

Alireza Razmavar, Gurubalan Annadurai, Adesola Olufade, and Carey J. Simonson

I am requesting the permission to use the contents of this manuscript of my M.Sc. thesis and all subsequent revisions that may be prepared at the University of Saskatchewan. Please indicate your agreement by signing below:

Sincerely,
Alireza Razmavar
October 1, 2021

Permission granted by: Carey J. Simonson
Signature:
Date:

A.2. PERMISSION FOR MANUSCRIPT USED IN CHAPTER 3

The manuscript presented in Chapter 3 is unpublished and therefore a copyright permission is obtained from all the co-authors of the manuscript which is included below:

Copyright Permission Request Form

I prepared a manuscript titled "A theoretical study on crystallization fouling limits in liquid-to-air membrane energy exchangers" to be published as the third chapter of my M.Sc. thesis and submitted to the Department of Mechanical Engineering at the University of Saskatchewan. The authors who contributed to this manuscript are

Alireza Razmavar, Gurubalan Annadurai, Adesola Olufade, and Carey J. Simonson

I am requesting the permission to use the contents of this manuscript of my M.Sc. thesis and all subsequent revisions that may be prepared at the University of Saskatchewan. Please indicate your agreement by signing below:

Sincerely,
Alireza Razmavar
October 1, 2021

Permission granted by: Gurubalan Annadurai
Signature:
Date:

Copyright Permission Request Form

I prepared a manuscript titled "A theoretical study on crystallization fouling limits in liquid-to-air membrane energy exchangers" to be published as the third chapter of my M.Sc. thesis and submitted to the Department of Mechanical Engineering at the University of Saskatchewan. The authors who contributed to this manuscript are

Alireza Razmavar, Gurubalan Annadurai, Adesola Olufade, and Carey J. Simonson

I am requesting the permission to use the contents of this manuscript of my M.Sc. thesis and all subsequent revisions that may be prepared at the University of Saskatchewan. Please indicate your agreement by signing below:

Sincerely,
Alireza Razmavar
October 1, 2021

Permission granted by: Adesola Olufade
Signature:
Date:

Copyright Permission Request Form

I prepared a manuscript titled "A theoretical study on crystallization fouling limits in liquid-to-air membrane energy exchangers" to be published as the third chapter of my M.Sc. thesis and submitted to the Department of Mechanical Engineering at the University of Saskatchewan. The authors who contributed to this manuscript are

Alireza Razmavar, Gurubalan Annadurai, Adesola Olufade, and Carey J. Simonson

I am requesting the permission to use the contents of this manuscript of my M.Sc. thesis and all subsequent revisions that may be prepared at the University of Saskatchewan. Please indicate your agreement by signing below:

Sincerely,
Alireza Razmavar
October 1, 2021

Permission granted by: Carey J. Simonson
Signature:
Date: